Probabilistic Hazard Assessment for Tornadoes, Straight-line Wind, and Extreme Precipitation at the Savannah River Site

D. Werth, A. Weber, and G. Shine

November, 2013

SRNL-STI-2013-00664

DISCLAIMER

Printed in the United States of America

Prepared for
U.S. Department of Energy

Probabilistic Hazard Assessment for Tornadoes, Straight-line Wind, and Extreme Precipitation at the Savannah River Site

D. W. Werth, A. H. Weber, and E. P.
Shine

November, 2013

Savannah River National Laboratory ™

OPERATED BY SAVANNAH RIVER NUCLEAR SOLUTIONS

REVIEWS AND APPROVALS

AUTHORS:

_____
D. W. Werth, Atmospheric Technologies Group   Date

_____
A. H. Weber, Atmospheric Technologies Group   Date

_____
E. P. Shine, Computational Engineering and Statistics   Date

TECHNICAL REVIEW:

_____
B. Viner, Atmospheric Technologies Group   Date

APPROVAL:

_____
C. H. Hunter, Atmospheric Technologies Group   Date

EXECUTIVE SUMMARY

Recent data sets for three meteorological phenomena with the potential to inflict damage on SRS facilities - tornadoes, straight winds, and heavy precipitation - are analyzed using appropriate statistical techniques to estimate occurrence probabilities for these events in the future. Summaries of the results for DOE-mandated return periods and comparisons to similar calculations performed in 1998 by Weber, et al., are given.

Using tornado statistics for the states of Georgia and South Carolina, we calculated the probability per year of any location within a 2° square area surrounding SRS being struck by a tornado (the 'strike' probability) and the probability that any point will experience winds above set thresholds. The strike probability was calculated to be 1.15E-3 (1 chance in 870) per year and wind speeds for DOE mandated return periods of 50,000 years, 125,000 years, and 1E+7 years (USDOE, 2012) were estimated to be 136 mph, 151 mph and 221 mph, respectively. In 1998 the strike probability for SRS was estimated to be 3.53 E-4 and the return period wind speeds were 148 mph every 50,000 years and 180 mph every 125,000 years. A 1E+7 year tornado wind speed was not calculated in 1998; however a 3E+6 year wind speed was 260 mph. The lower wind speeds resulting from this most recent analysis are largely due to new data since 1998, and to a lesser degree differences in the models used.

By contrast, default tornado wind speeds taken from ANSI/ANS-2.3-2011 are somewhat higher: 161 mph for return periods of 50,000 years, 173 mph every 125,000 years, and 230 mph every 1E+7 years (ANS, 2011). Although the ANS model and the SRS models are very similar, the region defined in ANS 2.3 that encompasses the SRS also includes areas of the Great Plains and lower Midwest, regions with much higher occurrence frequencies of strong tornadoes.

The SRS straight wind values associated with various return periods were calculated by fitting existing wind data to a Gumbel distribution, and extrapolating the values for any return period from the tail of that function. For the DOE mandated return periods, we expect straight winds of 123 mph every 2500 years, and 132mph every 6250 years at any point within the SRS. These values are similar to those from the W98 report (which also used the Gumbel distribution for wind speeds) which gave wind speeds of 115mph and 122 mph for return periods of 2500 years and 6250 years, respectively.

For extreme precipitation accumulation periods, we compared the fits of three different theoretical extreme-value distributions, and in the end decided to maintain the use of the Gumbel distribution for each period. The DOE mandated 6-hr accumulated rainfall for return periods of 2500 years and 6250 years was estimated as 7.8 inches and 8.4 inches, respectively. For the 24-hr rainfall return periods of 10,000 years and 25,000 years, total rainfall estimates were 10.4 inches and 11.1 inches, respectively. These values are substantially lower than comparable values provided in the W98 report. This is largely a consequence of the W98 use of a different extreme value distribution with its corresponding higher extreme probabilities.

TABLE OF CONTENTS

LIST OF TABLES

Table 5.7 Data for the annual maxima for the 3-hour accumulated precipitation.

Table 5.8 Data for the annual maxima for the 6-hour accumulated precipitation.

Table 5.9 Data for the annual maxima for 24-hour accumulated precipitation.

Table 5.9 continued.

Table 5.10 Peak precipitation values (inches) for DOE-mandated return periods.

LIST OF FIGURES

Figure 3.1 a) Map of tornado occurrences in Georgia, and South Carolina for F/EF0 (green), and F/EF1 (red) for the period 1950-2011. The black box indicates the 2^0 x 2^0 domain centered at the SRS.

Figure 3.1 b) Map of tornado occurrences in Georgia, and South Carolina for F/EF2 (orange) and F/EF3 (blue) for the period 1950-2011. The black box indicates the 2^0 x 2^0 domain centered at the SRS.

Figure 3.1 c) Map of tornado occurrences in Georgia, and South Carolina for F/EF4 (open) for the period 1950-2011. The black box indicates the 2^0 x 2^0 domain centered at the SRS.

Figure 3.2 Number of tornadoes from 1950-2011 in the two-state (Georgia and South Carolina) domain for the NCDC (blue) and the SPC (red) databases per year for the a) F0, b) F1, c) F2 before 2007, after which the respective number of EF tornadoes is shown.

Figure 3.2 Number of tornadoes from 1950-2011 in the two-state (Georgia and South Carolina) domain for the NCDC (blue) and the SPC (red) databases per year for the d) F3, e) F4 before 2007, after which the respective number of EF tornadoes is shown. No F5 or EF5 tornadoes occurred in either record.

Figure 3.3 Total area covered by each a) F and b) EF category for the NCDC and SPC databases within the two-state area (Georgia and South Carolina).

Figure 3.4 Schematic of the relative areas within a typical F2 tornado that experience EF0 or greater winds.

Figure 3.5 Total area covered by each category for the raw SPC data, and corrected for misclassification for the a) F-rated and b) EF-rated tornadoes.

Figure 3.6 Total area covered by each category for the raw SPC data (blue), and for data calculated using the lognormal expectation value (red) for the a) F-rated and b) EF-rated tornadoes.

Figure 3.7 a) The probability a point within a tornado path will have winds (3 second gust) at the given velocity, given that a strike occurs, b) the cumulative probability that any point within a strike will experience winds *above* that threshold, c) the probability (per year) that any point will experience winds at or above the given threshold.

Figure 3.8 Tornadic wind speeds for the 2^0 x 2^0 domain corresponding to various return periods for both the values calculated from the observed tornadic wind speeds (with Eqs.1-4) (3 second gust), for a linear extrapolation of those values, and values from the ANS-2.3-2011 report.

Figure 4.1 a) Annual wind gust maxima each year at Augusta, GA (NWS). b) As in a) but rendered nondimensional with the mean removed and normalized by the standard deviation (Eq. 7).

Figure 4.2 Ranked values of normalized wind maxima τ_{ij}.

Figure 4.3 a) Nonexceedance probability curves for a Frechet ($\kappa < 0$), Gumbel ($\kappa = 0$), and reverse Weibull ($\kappa > 0$) distribution. b) As in a), but above the 90th percentile. c) Return values for the three distributions.

Figure 4.4 Comparison of the actual wind data distribution with the a) Gumbel and b) Frechet distributions.

Figure 4.5 Comparison of the LHS and RHS of Eq. 15 for a) the Gumbel distribution, and b) the Frechet distribution.

Figure 4.6 Projected wind gust values for various return periods at SRS (from Eq. 21), along with the values from the W98 and the ANS-2.3-2011 reports.

Figure 4.7 Comparison of tornadic and straight wind gust probabilities.

Figure 5.1 a) Time series of annual maximum 15-minute precipitation readings for CLM for 1979. b) The same series, now aggregated to 1 hour accumulation periods.

Figure 5.2 Projected 15-minute precipitation totals for various return periods at SRS, along with values from the W98 report.

Figure 5.3 Projected 1 hour accumulation totals for various return periods at SRS, along with values from the W98 report.

Figure 5.4 Projected 3 hour precipitation totals for various return periods at SRS, along with values from the W98 report.

Figure 5.5 Projected 6 hour precipitation totals for various return periods at SRS, along with values from the W98 report.

Figure 5.6 Projected 24 hour precipitation totals for various return periods at SRS, along with values from the W98 report.

LIST OF SYMBOLS

F/EF	Fujita/Enhanced Fujita rating
a(F,i)	Area of the ith tornado of magnitude F
A(F)	Total area covered by tornadoes of rating F
FR(EF,F)	The fraction of the area of an F scale tornado that is reallocated as EF wind speed
P_{strike}	Strike probability
A_T	Total area covered by tornadoes
A_R	Total area of domain
N_{year}	Number of years of tornado record
N_F	Number of tornadoes of rating F
Awind(EF)	Total area covered by wind speeds of rating EF
u(F)	log mean of the area covered by tornadoes of rating F (dimensionless)
v(F)	log variance of the area covered by tornadoes of rating F (dimensionless)
E(F)	lognormal area covered by tornadoes of area F (km^2)
X_{ij}	Annual maximum wind gust/rainfall at station j in year i
$\bar{X}_j$	Multi-year average of X_{ij} at station j
s_j	Multi-year standard deviation of X_{ij} at station j
τ_{ij}	Standardized value of annual maximum wind gust/rainfall at station j in year i

k   Number of stations

n_T Total number of observations of all the stations

n_j Number of years of data at station j

κ Shape parameter

α Scale parameter

ξ Location parameter

p   nonexceedance probability

RP_{τ_p} Return period

τ_P Value of τ corresponding to return period P.

CV   Coefficient of variation

X_{pj} Annual maximum wind gust/precipitation associated with return

                           period p at station j

LIST OF ABBREVIATIONS

ANS American Nuclear Society

ATG Atmospheric Technologies Group

CDF cumulative distribution function

CLM Central Climatology Site

DOE Department of Energy

EF Enhanced Fujita Scale

F Fujita Scale

NCDC National Climatic Data Center

NWS National Weather Service

PHA Probabilistic Hazard Assessment

PNNL Pacific Northwest National Laboratory

PWM probability weighted moments

SPC Storm Prediction Center

SRNL Savannah River National Laboratory

SRS Savannah River Site

1.0 Introduction

The Savannah River National Laboratory (SRNL) Atmospheric Technologies Group (ATG) has performed an update to the Probabilistic Hazard Assessment (PHA) for severe weather phenomena at the Savannah River Site (SRS), in accordance with Department of Energy Standard DOE-STD-1020-2012 (USDOE, 2012), Section 4.3.2.1. The PHA is to estimate future risk from three natural hazards – tornadoes, extreme straight winds, and extreme precipitation. In each case, the general theory is the same – the probabilities for the future are to be calculated from the statistics of the past. This is relatively simple for events that happen often (e.g., a daily rainfall greater than of 0.25"), but it is also necessary to calculate the probabilities of events that are rare, or even that have yet to happen, which is more challenging. To accomplish this, ATG collected existing datasets of the three phenomena to quantify the occurrence probabilities of extreme events, which are uncommon and therefore difficult to quantify based on their observed frequencies of occurrence. This involved the application of existing statistical techniques to newer datasets.

Such a report was produced previously by Weber et al., (1998, henceforth W98). For straight wind and precipitation, the same statistical methods are applied to newer, larger datasets. For tornadoes, however, we will apply newer techniques as per DOE-STD-1020-2012 and ANS 2.3-2011. Our results will be compared to those of W98, and significant differences discussed.

2.0 Site Characterization

The following discussion is provided in accordance with requirements summarized in DOE-STD-1020-2012, Section 4.2.

2.1 General Climate

The following SRS climate summary is taken from Scott (2013) and WSRC (2004). The Savannah River Site region has a humid subtropical climate characterized by relatively short, mild winters and long, warm, humid summers. Summer-like conditions typically last from May through September, when the area is frequently under the influence of a western extension in the semi-permanent Atlantic subtropical anticyclone (i.e. the 'Bermuda' high). Winds in summer are light and cold fronts generally remain well north of the area. Scattered afternoon and evening thunderstorms are common. The remnants of tropical storms and hurricanes affect the area every few years.

The influence of the Bermuda high begins to diminish during the fall, resulting in lower humidity and more moderate temperatures. Average rainfall during the fall is usually the least of the four seasons.

In the winter months, mid-latitude low pressure systems and associated fronts often migrate through the region. As a result, conditions frequently alternate between warm, moist, subtropical air from the Gulf of Mexico region and cool, dry polar air. The Appalachian Mountains to the north and northwest of the SRS help to moderate the extremely cold temperatures that are associated with occasional outbreaks of Arctic air into the U.S. Consequently, less than one-third of winter days have minimum

temperatures below freezing on average, and days with temperatures below 20°F are infrequent. Observed temperature extremes at SRS range from a maximum of 107 F (July, 1986) to a minimum of -3° F (January, 1985).

Tornadoes occur more frequently in spring than the other seasons of the year. Although spring weather is somewhat windy, temperatures are usually mild and humidity is relatively low.

Ten tornadoes have occurred on or in close proximity to the SRS since operations began in the 1950s. Four F-2 tornadoes struck forested areas of SRS on three separate days during March 1991. Considerable damage to trees was observed in the affected areas. A tornado that occurred during October 1989 knocked down several thousand trees over a 16-mile path across the southern and eastern portions of the site. Wind speeds produced by this F-2 tornado were estimated by the National Weather Service (NWS) to be as high as 150 mph. An additional four confirmed tornadoes were classified as F-1 and produced relatively minor damage. The most recent occurrence of a tornado was in November 2011, when an EF0 tornado touched down near D-area and continued northeastward, causing minor damage in N-area. None of the ten tornadoes on site caused significant damage to structures.

Because the SRS is approximately 100 miles inland, winds associated with tropical weather systems usually diminish below hurricane force. However, winds associated with Hurricane Gracie, which passed to the north of SRS on September 29, 1959, were measured as high as 75 mph on an anemometer located in F-Area. No other hurricane-

force wind has been measured on the site. On September 22, 1989, the center of Hurricane Hugo passed about 100 miles northeast of SRS. The maximum 15-minute average wind speed observed onsite during this hurricane was 38 mph. The highest observed instantaneous gust was 62 mph. The data were collected from the onsite tower network (measurements taken at 200 feet above ground). Extreme rainfall and tornadoes, which frequently accompany tropical weather systems, usually have the most significant hurricane-related impact on SRS operations.

The annual average precipitation at SRS is 47.2 inches. The range of annual rainfall over the period from 1952 was from 73.5 inches (1964) to 28.8 inches (1954). A total of 19.6 inches was recorded at SRS in October, 1992. Of this total, 10.2 inches fell in a 48 hr period during the passage of two tropical storms. Heavy rainfalls over short durations are typically associated with slow moving thunderstorms. Rainfall amounts greater than 5 inches in less than 12 hours have been observed on several occasions.

Measurable ice or snow occurs an average of once every 1-2 years. The greatest single snowfall recorded in the SRS area (Augusta, NWS) over the period 1949-2006 was in February 1973 when 13.7 inches fell in a 24-hour period. Total accumulation for that storm was 14.0 inches. Significant snowfalls typically melt within a day or two; consequently, heavy rain coincident with a persistent large snowpack would not be expected to occur in this region.

2.2 Onsite Meteorological Data Collection

The meteorological monitoring program at SRS is conducted in a manner fully consistent with the requirements of DOE Order 458.1, *Radiation Protection of the Public and the Environment* (USDOE, 2011) and ANSI/ANS-3.11-2010 (ANS, 2010) and DOE-EH/0173T (USDOE, 2004). This program is documented in the SRS Environmental Monitoring Plan (SRNS, 2012). The onsite data are collected from a network of nine primary monitoring stations. Towers located adjacent to each of eight operations areas (A, C, D, F, H, K, L, and P areas) are equipped to measure wind direction, wind speed, temperature, and dew point at a height of 61 meters (m) above ground. These towers are located within a forest canopy adjacent to the operations area to gather data representative of the prevailing surface that characterizes the Site.

A ninth tower near N-Area, known as the Central Climatology site (CLM), is instrumented with wind, temperature, and dew point sensors at four levels: 2m (4m for wind), 18m, 36m, and 61m. The CLM site is also equipped with an automated tipping bucket rain gauge, a barometric pressure sensor, and a solar radiometer near the tower at ground level. This tower is located in a flat, cleared area. Data from CLM are available since the early 1990s.

Data acquisition units at each station record a measurement from each instrument at 1-second intervals. Every 15 minutes, the 1-second data are processed to generate statistical summaries for each variable, including averages and instantaneous maxima, and the results are uploaded to a relational database for permanent archival.

Additional precipitation measurements are collected from a network of 12 plastic wedge rain gauges across the SRS. These gauges are read manually by security or operations personnel once per day, usually around 6 a.m. The daily data are reported each morning, reviewed to correct obvious flaws, and manually entered into a permanent electronic data base.

3.0 Probabilistic Hazard Assessment for Tornadoes

3.1 Tornado Data

Unlike many weather variables such as temperature, which can be recorded automatically, tornadoes are recorded through direct observation, and this often produces idiosyncrasies in tornado records. Different databases from equally credible sources may contradict one another, earlier records may show signs of being less accurate than later records within the same database, or tornado magnitudes may be simply misjudged. The latter is especially true, since tornado wind speeds are seldom measured directly and are instead estimated based on the damage inflicted on trees, buildings, etc. As we will see, these problems require adjustment to the data.

An important consideration is the domain over which the statistics are to be calculated. Datasets list tornadoes over the entire United States, but we wish to characterize the risk for the area near SRS. A domain too large (for example, encompassing parts of Oklahoma and Texas) will include data from areas that are unrepresentative of the tornado risk at SRS in South Carolina, and too small a domain will likely also produce unrepresentative results, with potential high magnitude tornadoes absent from the data.

We will look at two domains: the combined two-state area of Georgia and South Carolina, and a 2° x 2° box centered at SRS. The latter domain will be applied twice – for the same data used in W98 (which used that same domain), using the revised tornado risk model (described in Sec. 3.2), and again with a newer, updated dataset. A map of tornado touchdown points (Figure 3.1) reveals how northern and western Georgia tend to experience more tornadoes, with an area of generally lower frequency stretching from east central Georgia into western South Carolina. The map also reveals that no F5 or EF5 tornadoes have been recorded in Georgia or South Carolina, though a few have hit in Alabama.
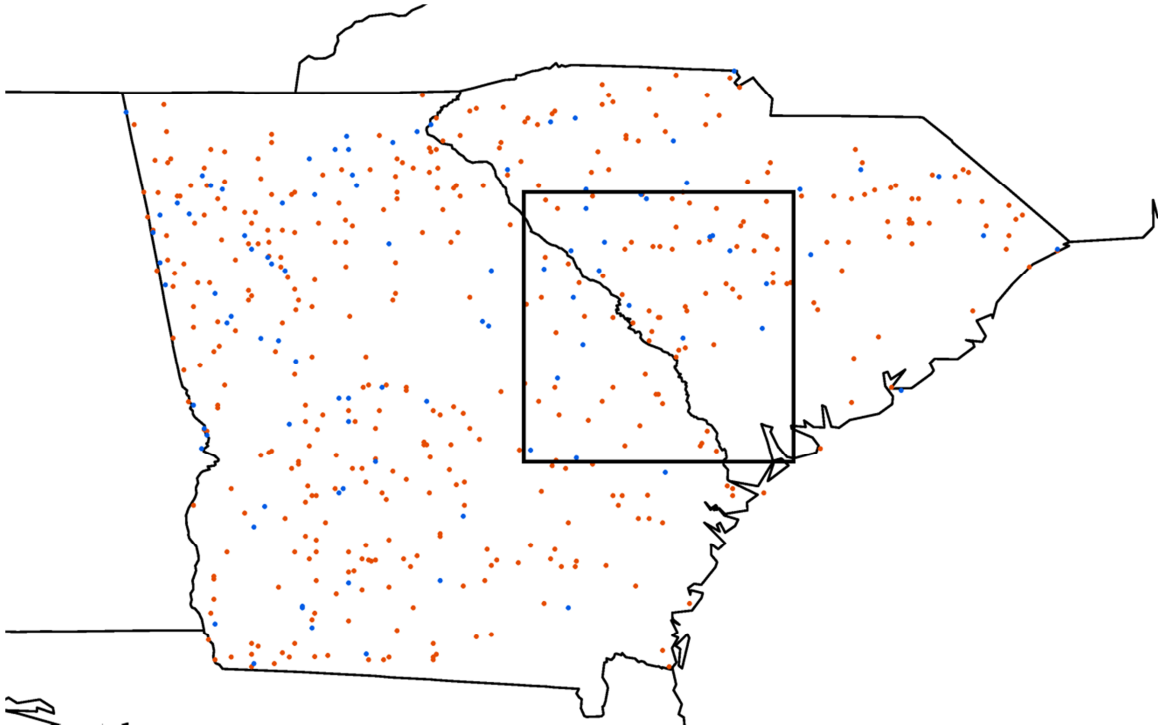
Figure 3.1 a) Map of tornado occurrences in Georgia, and South Carolina for F/EF0 (green), and F/EF1 (red) for the period 1950-2011. The black box indicates the 2° x 2° domain centered at the SRS.
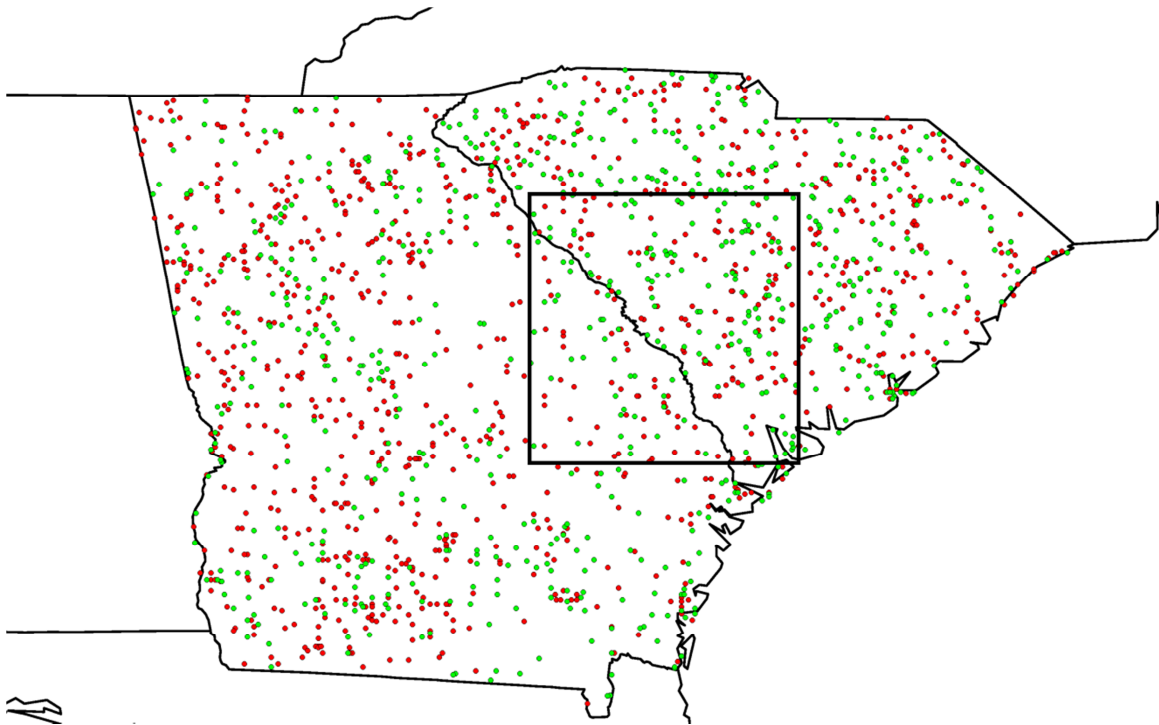
Figure 3.1 b) Map of tornado occurrences in Georgia, and South Carolina for F/EF2 (orange) and F/EF3 (blue) for the period 1950-2011. The black box indicates the 2⁰ x 2⁰ domain centered at the SRS

Figure 3.1 c) Map of tornado occurrences in Georgia, and South Carolina for F/EF4 (open) for the period 1950-2011. The black box indicates the 2⁰ x 2⁰ domain centered at the SRS.

Another consideration is the scale used to classify tornado intensity – in 2007, the Fujita scale (F-scale) was replaced with the Enhanced Fujita-scale (EF-scale), which was judged to be more accurate for assigning wind speed based on the observed damage. These scales assign different wind speeds to their respective 0-5 categories; for example, an F2 represents winds from 118mph to 161mph, while an EF2 has winds from 111mph to 135mph. When calculating the numbers or cumulative damage areas of the different types, we must take care to maintain separate groupings for the F-rated and EF-rated tornadoes.

Several relatively complete datasets exist, and we looked at two – the Storm Prediction Center (SPC) tornado database, and a storm database maintained by the National Climatic Data Center (NCDC) – to compare them and select one for analysis. Both datasets contain information on the date, magnitude, length and width of all recorded tornadoes, all required by DOE-STD-1020-2012, Section 4.2.3.2.3. Both also list the state and county, but the SPC dataset has one major advantage - it lists the latitude and longitude of each tornado touchdown and liftoff point, allowing for an easier filtering of tornadoes by location. (NCDC lists tornadoes by county, making such filtering more difficult.)

A line-by-line comparison of the two datasets reveals much similarity, but also several instances in which a tornado in the SPC dataset is reported as two separate tornadoes in the NCDC dataset (Table 3.1a). A time series of the number of reported F-scale

tornadoes (before 2007) and EF-scale tornadoes (starting in 2007) over the two-state area

per year (Fig. 3.2) reveals that this major difference in the number of recorded tornadoes

a)

year	month	day	Length (mi)	Width (yds)
1952	1	22	0	33
1952	1	22	1.9	350
1952	1	22	6.8	350

year	month	day	Length (mi)	Width (yds)
1952	1	22	8.7	350
1952	1	22	0.1	10

b)

year	month	day	Length (mi)	Width (yds)
1951	6	8	0	100
1951	6	24	0	33
1951	11	15	0	150

year	month	day	length (mi)	Width (yds)
1951	6	8	0.1	100
1951	6	24	0.1	10
1951	11	15	0.1	150

Table 3.1 a) Selection of January tornado (for illustration) data for NCDC (top) and SPC (bottom), b) as in a) but for June/November.

between the datasets is greatest at the larger F/EF scale values, with correspondingly

fewer reported tornadoes in the SPC database of all F/EF classes except F0/EF0 (Table

3.2). This by itself would not affect the results (so long as the recorded magnitude is the

same), since the total tornado area is the statistic we will use to estimate tornado strike

probabilities, and this is the same whether the same area is subdivided into a large

number of small areas or a smaller number of larger areas. Many tornadoes in the NCDC

database are listed with zero length (Table 3.1b), which would result in a zero calculated

area. Therefore, the total area affected by each magnitude:

$$A(F) = \sum_{i=1}^{N_F} a(F, i) \tag{1}$$
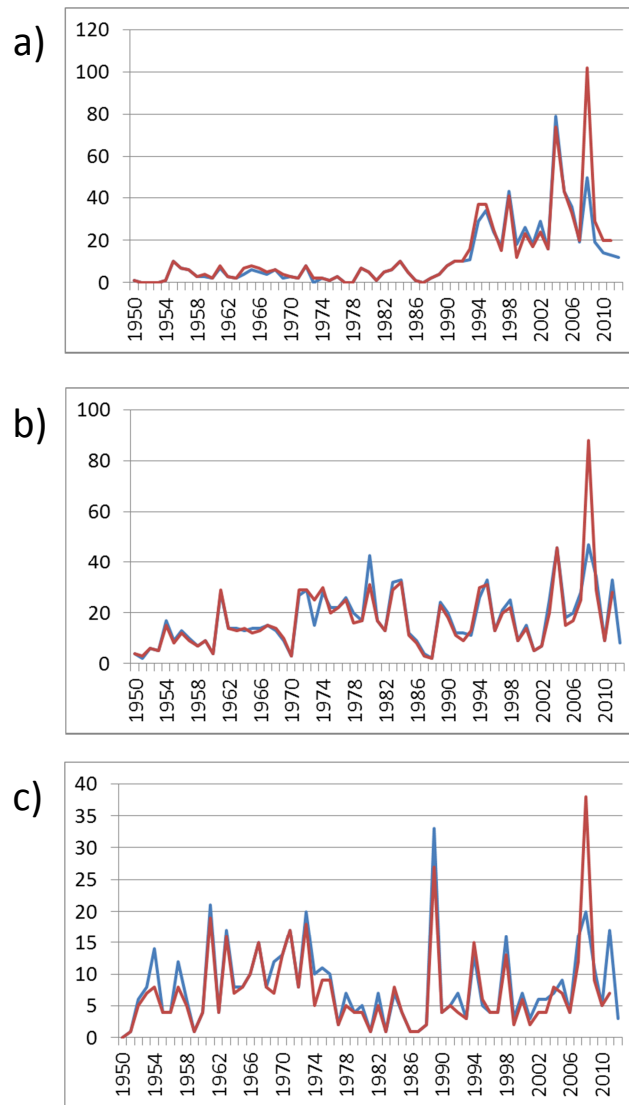
Figure 3.2 Number of tornadoes from 1950-2011 in the two-state (Georgia and South Carolina) domain for the NCDC (blue) and the SPC (red) databases per year for the a) F0, b) F1, c) F2 before 2007, after which the respective number of EF tornadoes is shown.

d)

e)
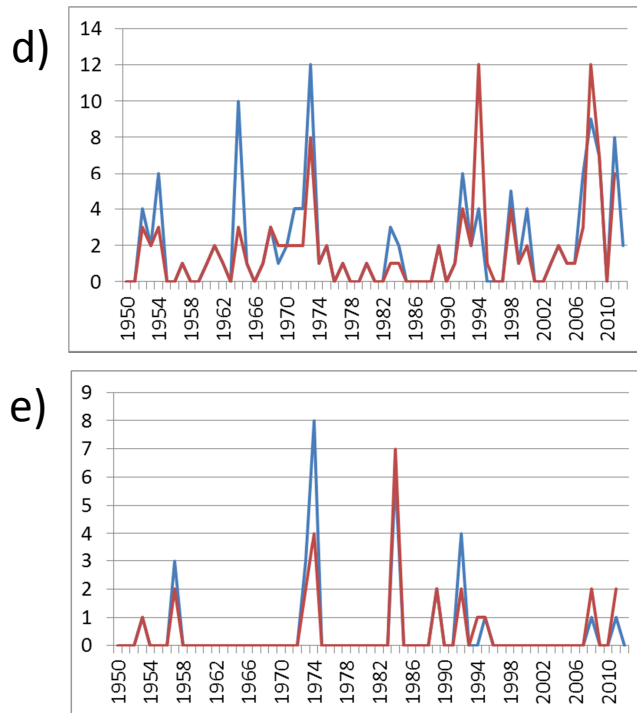
Figure 3.2 Number of tornadoes from 1950-2011 in the two-state (Georgia and South Carolina) domain for the NCDC (blue) and the SPC (red) databases per year for the d) F3, e) F4 before 2007, after which the respective number of EF tornadoes is shown. No F5 or EF5 tornadoes occurred in either record.

	NCDC	SPC
F0/EF0	715	783
F1/EF1	1095	1080
F2/EF2	505	451
F3/EF3	127	106
F4/EF4	30	26

Table 3.2 Number of tornadoes (between 1950-2011) of each magnitude recorded over Georgia and South Carolina in the NCDC and SPC datasets.

where $a(F,i)$ is the area of the ith tornado of magnitude F in square kilometers (for data after 2007, F in Eq. 1 is replaced by EF), and N_F is the total number of F tornadoes, shows much larger values for the SPC data (Fig. 3.3), which will ultimately yield a greater strike probability. We elected to use the SPC data, given its more complete indexing of the tornado history.
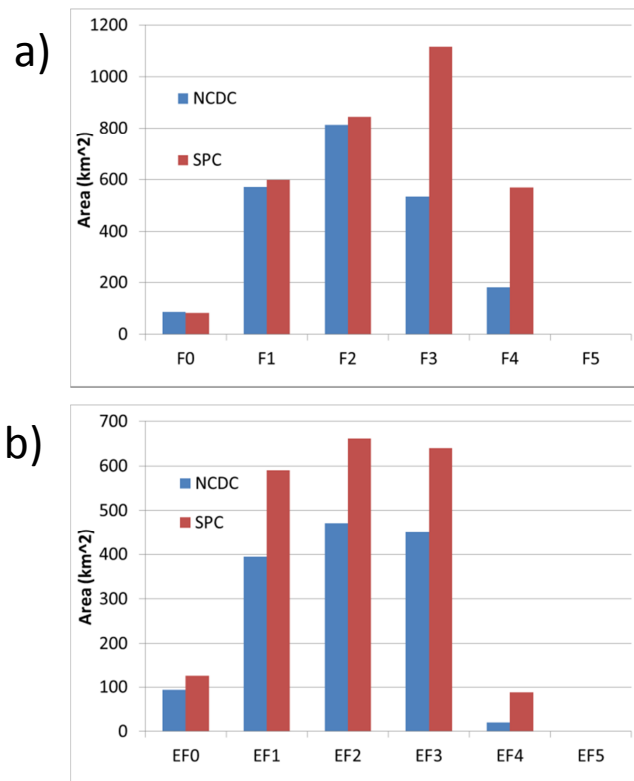
Figure 3.3 Total area covered by each a) F and b) EF category for the NCDC and SPC databases within the two-state area (Georgia and South Carolina).

3.2 Tornado Risk Model

a. Probability

An algorithm for calculating the future probability of experiencing tornadic winds above

a set threshold was outlined by Ramsdell et al., (2007, henceforth R07) in their report on

the PHA for the Pacific Northwest National Laboratory (PNNL). DOE criteria and

guidance contained in 2012 (DOE-STD-1020-2012) specify in Section 4.3.2.5 that the

sites utilize section 3.4 of the American Nuclear Society (ANS) ANS-2.3-2011 for the

criteria and guidance on developing their site PHA, and that standard lists R07 as one of

two acceptable sources for an algorithm to estimate probabilities of tornadic winds. The

other was developed by Lawrence Livermore National Laboratory (LLNL) (Boissonnade

et al., 2000). For SRS purposes, the PNNL algorithm appears to be more appropriate

(though similarities exist between the two), mostly because it is fundamentally similar to that of W98, thus providing some continuity of approach, requires less manipulation to the data, and served as the basis for the ANS-2.3-2011 standard (Section 3.4). Unlike the LLNL report, the PNNL algorithm does not require the calculation of multiple distribution functions for tornado touchdown location, direction, length and width or the use of 'expert judgment' to decide on the best parameters for those distributions (e.g., the smoothing parameters to convert tornado locations to a continuous function). Instead, the PNNL algorithm uses the actual statistics more directly, and does not require any special software (LLNL made use of a model that is not publicly available). Therefore, most of the description below is based on the PNNL model.

Tornado risk assessments start with two premises – the probability per year of any location within a larger domain being struck by a tornado (P_{strike}) is related to the area within the domain that has been struck in the past (R07; Boissonnade et al., 2000; W98), and the probability of any tornado having winds above certain thresholds is related to the distribution of tornado magnitudes that have occurred (R07, W98). For the first, R07 writes this simply as:

$$P_{strike} = \frac{A_T}{N_{year} A_R} \tag{2}$$

in which N_{year} is the number of years of the record, A_R is the total area of the domain of interest, and

$$A_T = \sum_{F=0}^{5} A(F) \tag{3}$$

is the total area struck by all tornadoes during the period of record. Given that the area affected by each tornado in the SPC database is provided, we can calculate P_{strike}.

For the second premise, R07 states that the probability of a point within a tornado path experiencing winds above a certain threshold is not uniform, but is proportional to the area within each tornado path above that threshold (Fig. 3.4). Tornadoes are classified according to the peak intensity, and a tornado will often evolve through several F/EF wind speed values between touchdown and dissipation. Therefore, a tornado path will comprise areas that experienced different wind speeds, with only a small fraction of the total area actually seeing the highest speeds (Fig. 3.4). Starting with the work of Reinhold and Ellingwood (1982), who calculated the fractions of an F-scale reported tornado area that experienced various F-scale wind speeds, R07 calculates a table (Table 3.1 of R07, reproduced here as Table 3.3) that is used to calculate what fraction FR(EF,F) of each F-reported area A(F) is covered by winds of EF magnitude (A_{wind}(EF)):

$$A_{wind}(EF) = \sum_{F=0}^{5} A(F) FR(EF, F) \qquad (4)$$

For example, an F2 tornado area is partitioned as having about 62% of its total area within the EF0 wind speed range, 27% within the EF1 range, and 12% in the EF2 range (Fig. 3.4), while an F0 tornado is entirely within the EF0 range. Assuming uniform strike probability (calculated using Eq. 2) within the selected domain, and the probability that each strike will yield winds of various magnitudes calculated with FR(EF,F), we can calculate the probability per year of any point experiencing tornadic winds above a threshold as a product of the two.

Recorded Tornado F scale

Intensity EF Scale		F0	F1	F2	F3	F4	F5
	EF0	1	0.772	0.616	0.529	0.543	0.538
	EF1		0.228	0.268	0.271	0.238	0.223
	EF2			0.115	0.133	0.131	0.119
	EF3				0.067	0.056	0.07
	EF4					0.032	0.033
	EF5						.017

Table 3.3 Tornado Area Intensity Distribution for the Point Structure Design Wind Speed Estimates (from R07).
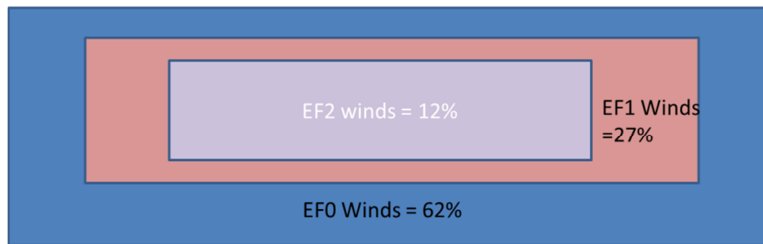
Figure 3.4 Schematic of the relative areas within a typical F2 tornado that experience EF0 or greater winds.

A different model (Lu, 1995 and McDonald, 1981) was followed in the W98 report. That model relies on a "occurence-intensity" distribution for the area of applicability. When this distribution was compiled for the two-degree square surrounding SRS it was found that there were no F-5, two F-4, and eight F-3 tornadoes, i.e, the two-degree box was under-represented for the more severe tornadoes compared to larger boxes drawn for the region. A decision was made by the authors that a more accurate representation of the area-intensity relationship would need to include the stronger tornadoes from the states of South Carolina, Georgia, and Alabama. Ultimately, all F-3 and F-4 tornadoes that

16

occurred in Georgia and South Carolina and all F-4 and F-5 tornades that occured in Alabama were included as well as all the F-0, F-1, and F-2 tornadoes within the two-degree square between 1951 through 1996 to determine the "occurence-intensity" tornado distribution used in W98. We will compare the results of that analysis with those from the current report.

b. Data Processing

Correction for Tornado Misclassification

As stated previously, tornado magnitudes are estimated subjectively, given the degree of the damage. Any tornado dataset must therefore address tornado misclassification – instances in which observers estimate (and record) a tornado as being of one magnitude when in reality another would be more appropriate. A process for correcting the database for misclassification was developed by Lu (1995), who assumed that the tornado magnitude can be represented as a continuous, normally distributed variable, with a degree of overlap between categories. The estimated area of overlap allows for the calculation of a probability matrix that a tornado recorded at one magnitude should be reclassified as another (Table 3.4). An example is shown in Fig. 3.5 for both the F and EF tornado areas, where some of F/EF1-3 tornado areas have been reassigned to the F/EF0, 4, and 5 categories. This same process was applied by W98, and we elected to apply it to our calculated tornado areas as well. Note that, after the correction for misclassification, category 5 tornado data now exists in the record, and this will be used to estimate the probability of F (or EF) category storms occurring in the future. This is the sole source of F5 and EF5 tornadoes in our two-state record.

Recorded F Value

Corrected Fraction		0	1	2	3	4	5
	0	0.8413	0.1574	0.0013	0	0	0
	1	0.1574	0.6826	0.1574	0.0013	0	0
	2	0.0013	0.1574	0.6826	0.1574	0.0013	0
	3	0	0.0013	0.1574	0.6826	0.1574	0.001
	4	0	0	0.0013	0.1574	0.6826	0.157
	5	0	0	0	0.001	0.159	0.841

Table 3.4 Matrix to reassign recorded F tornado areas to corrected F categories. (from Lu (1995)).
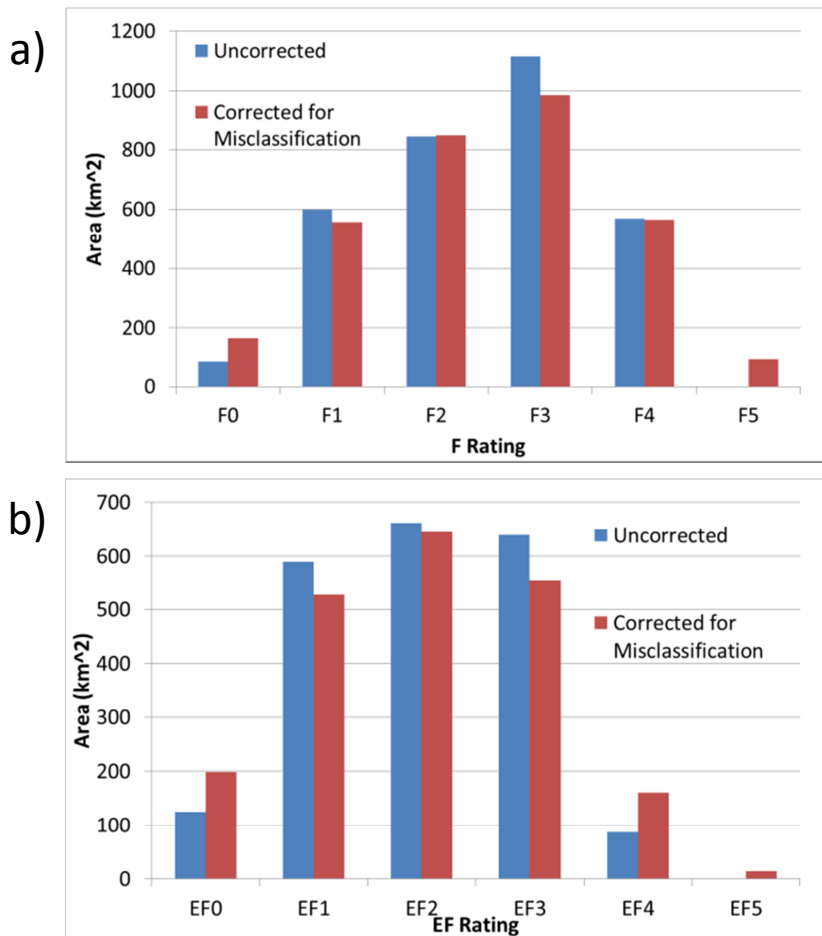
Figure 3.5 Total area covered by each category for the raw SPC data, and corrected for misclassification for the a) F-rated and b) EF-rated tornadoes.

18

Calculation of Total Tornado Area

The best way to calculate the total area covered by each F/EF category must also be considered. This can be done by simply adding the areas of the individual tornadoes (an arithmetic mean). R07, however, points out that it would be more accurate to assume that the tornado areas in the database do not constitute the entire 'universe' of tornado data, but were instead drawn from a lognormal distribution that accurately describes that universe. If we use the existing data to calculate the properties of that distribution, we could get a more accurate 'expectation value'. Simply assuming that the arithmetic average is a good value to use as the expectation value can result in a negatively biased tornado area.

R07 summarizes the procedure to estimate the expected area E(F) for each F category. Assuming areas are lognormally distributed, the logarithm of the area is normally distributed within category F. If we first take the natural logarithm of each tornado area $a(F,i)$ in category F, then get the mean u(F) and variance v(F) of that normally distributed variable:

$$u(F) = \frac{1}{N_F}\sum_{i=1}^{N_F} \ln(a(F,i)) \tag{5a}$$

$$v(F) = \frac{1}{N(F)-1}\sum_{i=1}^{N_F}(\ln(a(F,i)) - u(F))^2 \tag{5b}$$

then the mean area, E(F), is calculated as:

$$E(F) = e^{(u(F)+\frac{v(F)}{2})} \tag{6}$$

This quantity, multiplied by the number of tornadoes in category F, is used to get a more accurate value of the total area A(F). Applied to the SPC data, we get a new distribution of areas A(F) (Fig. 3.6) that is quite different from the original distribution. Not only are

the total areas using the lognormal distribution larger than the total areas using the arithmetic mean, but the distribution is skewed more to the larger magnitudes.
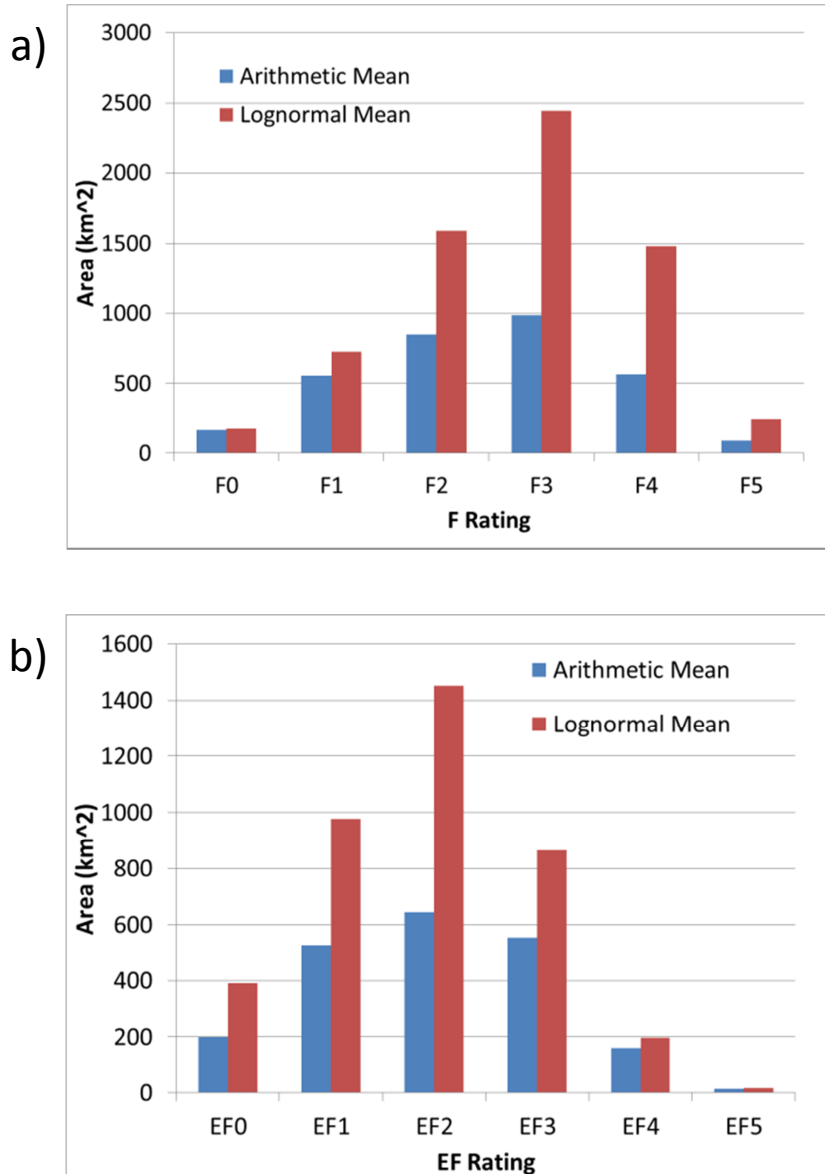
Figure 3.6 Total area covered by each category for the raw SPC data (blue), and for data calculated using the lognormal expectation value (red) for the a) F-rated and b) EF-rated tornadoes.

Correction for Reporting Bias

Changes in the observing networks, methods, and practices over time will lead to changes in the data that are recorded. The trend in F0/EF0 tornado occurrence after 1990 (Fig. 3.2) suggests that these tornadoes were often missed in the past, and only in the later years do the reports capture their true statistics. R07 outlines a simple procedure to correct for this – assume that the statistics of the later years are representative of the entire interval, and adjust the values of E(F=0) (and A(F=0)) accordingly.

A Student's t-test reveals that the mean for only the number of F0 tornadoes reported in the last 8 years of F-scale recording (1999-2006, the last 8 years that scale was applied) is significantly different from the previous years at an α= 1% level of significance[1] (and the other categories were not), so we will apply this adjustment to only that category - for F=0, u(F) and v(F) are calculated only with data from 1999-2006 and E(0) is calculated as in Eq. 6. The number of F0 tornadoes is similarly rescaled for the entire 57-year record – the number that occurred from 1999-2006 is multiplied by 57/8, so that the average number per year for 1999-2006 is assumed to have occurred each year from 1950-1998.

Fig. 3.2 reveals that much of the 'increase' in F0 and F1 tornado activity has occurred since W98 was prepared. If we do correct for the trend as described above, we should see threshold probabilities higher than those calculated in the earlier report, if only because the data recorded in the interim would make tornado strikes more likely. To test

---

[1] The level of significance is only approximate, since the current and earlier groups were formed by examining the data.

this, we also will recalculate the PHA using only data prior to 1998 (from the W98 dataset) to estimate the effect of the new data.

Scale Conversion

To apply Table 3.3, we need a way to 'convert' each recorded EF-scale tornado area to a corresponding F-area. This is accomplished with the same method Lu (1995) applied to estimate the probability that a tornado recorded at one rating should actually be reclassified as another. We assume a probabilistic distribution for each EF category, centered at the category midpoint and with a standard deviation of 0.5. This is used to calculate the probability that winds within each EF category lie within the ranges of the F categories (Table 3.5). (For example, ~62% of the recorded EF0 area is reassigned as F1, while 38% is assigned as F0.)

EF Value

		0	1	2	3	4	5
	0	0.38	0.020675	0	0	0	0
	1	0.618	0.856	0.200	0.0057	0	0
F Value	2	.00011	.123	0.797	0.698	0.081	0.037
	3	0	0	0.0023	0.297	0.838	0.146
	4	0	0	0	0	0.08	0.325
	5	0	0	0	0	0	0.328

Table 3.5 Matrix to reassign recorded EF tornado areas to the F categories.

Recorded Path Width

Finally, an important change in the tornado recording protocol was implemented in 1994 – the path width was recorded as the maximum width, rather than the mean width that had been estimated earlier. This will manifest itself as larger tornado footprint areas in

later records, with correspondingly higher strike probabilities.   In keeping with R07, however, we elect to apply no correction to compensate for this, preferring to maintain conservative results.

The complete algorithm is outlined below, and is applied separately to three domains – 1) the two-state domain comprising Georgia and South Carolina using SPC data from 1950-2011, 2) the 1950-2011 period over a 2° x 2° domain centered at SRS using SPC data, and 3) the 1950-1998 period over a 2° x 2° domain centered at SRS, using the data from W98.

i) Calculate the mean $u(F)$, $u(EF)$, and variance $v(F)$, $v(EF)$ of the logarithm of the tornado areas within each F/EF category and count the number in each category N_F and N_{EF}. For F=0, only use the years 1999-2006 to get the means and variances.

ii) Calculate the expected tornado areas within each F/EF category according to Eq. 6, and the number of tornadoes within each F/EF category.

iii) For F=0, rescale the number of tornadoes $N_{F=0}$ by multiplying by 57/8.

iii) Calculate the total area of each category as $A(F) = E(F) \times N_F$, $A(EF) = E(EF) \times N_{EF}$.

iv) Apply the misclassification matrix (Table 3.4) to adjust the area of the different categories.

v) Apply the EF-F allocation matrix (Table 3.5) to the EF areas to rescale them.

These areas are then used in Eqs. 3 and 2 to get the annual strike probability, and in Eq. 4 to get the probability of each wind speed, given that a strike occurs. The product of these two is then used to calculate the annual probability of a point experiencing winds above a threshold.

3.3 Results for Tornadoes

For the two-state domain, the total affected area A_T is 10,848 km^2, and the total area of the two-state domain A_R is 236,840 km^2 (United States Census Bureau, 2000), with a record length of N_{year}=62 years. Eq. 2 therefore yields a strike probability of 7.39 x 10^{-4} per year (Table 3.6). A full 2° x 2° domain covers an area of about 41,200km^2, but W98 writes that the domain should exclude large water bodies or steep terrain, and therefore apply a slightly smaller area of 39907 km^2, which we will apply here as well. Within that domain, the value of A_T is 2,850km^2, for a larger strike probability of 1.15 x 10^{-3} (Table 3.6).

Data Set	Strike Probability
SPC Two-State Domain	7.39e-4
SPC 2° x 2° Domain	1.15e-3
W98 2° x 2° domain	4.72e-4

Table 3.6 Calculated strike probabilities (per year) for the three datasets.

Within the 2° x 2° domain, the SPC data has tornadoes occurring at a slightly higher frequency than the larger 2-state domain – the area of the latter is about six times larger, but has only five times the number of tornadoes in the record. This is largely due to the low-frequencies in coastal areas (Fig. 3.1b, c). The expected tornado areas for the smaller domain tend to be larger as well, implying that a single tornado in the 2° domain will cover a larger area than is typical for the 2-state domain. These two effects combine for the larger strike probability in the 2° domain.

The average number of tornadoes per year is little over two-thirds in the W98 data record as in the SPC database (note that the W98 record ends in 1996, just as the 'increase' in F0 tornado reports (Fig. 3.2) begins). The 46-year W98 record length is three-fourths of the 62-year SPC record, but the total area A_T for the W98 data is only 867 km^2, about one-fourth of the total area from the SPC dataset. Using a 2° x 2° domain area of 39,907 km^2, this results in a lower strike probability for the W98 data of 4.72 x 10^{-4} (Table 3.6). This is close to the value of P_{strike} given in the W98 report (3.53 x 10^{-4}), suggesting that the different algorithm applied in the current report is not the primary cause of the difference between the values calculated here with that of W98 (since the application of both algorithms to that data gives about the same result). Rather, it is the newer data since 1998 that is causing most of the difference.

Table 3.7a lists the probability of a point experiencing winds at each category, given that a strike occurs as determined by Eq. 4. With the data of W98, the probability is weighted towards the *higher* categories (Fig. 3.7a), with a tornado less likely to be an EF0 and more likely to be EF1-5 (relative to the SPC data). In keeping with Fig. 3.7a, cumulative probabilities for the W98 data fall off slower than those for the SPC dataset (Fig. 3.7b). At lower thresholds, the probability per year that any point within the domain will experience tornadic winds above a set threshold (Table 3.7b, Fig. 3.7c) is highest for the SPC data within the 2° x 2° domain, which has the highest strike probability. At the highest category (EF5), the W98 data, in which tornadoes are more likely to be F2-5, has the highest probability of occurrence. All three are relatively close, however.

	Wind Speed (mph, 3 s gust)	SPC 2-State domain	SPC 2° x 2° domain	W98 2° x 2° domain
a)	65	0.633	0.659	0.586
	86	0.241	0.239	0.253
	111	0.093	0.0808	0.113
	136	0.027	0.017	0.0386
	166	0.00519	0.0029	0.00877
	200	0.000392	0.00021	0.000695

	Wind Speed (mph, 3 s gust)	SPC 2-State domain	SPC 2° x 2° domain	W98 2° x 2° domain
b)	65	7.39E-04	1.15E-03	4.72E-04
	86	2.71E-04	3.92E-04	1.96E-04
	111	9.29E-05	1.17E-04	7.60E-05
	136	2.42E-05	2.36E-05	2.27E-05
	166	4.13E-06	3.60E-06	4.47E-06
	200	2.89E-07	2.45E-07	3.28E-07

Table 3.7 a) Probability of a point within a given tornado experiencing winds at the indicated speeds. b) Probability per year of a point within SRS experiencing winds above the indicated speeds.

The EF-speeds for the 2° x 2° domain are plotted against their respective return periods (Fig. 3.8), and an exponential fit (Fig. 3.8) shows the winds associated with *any* return period (Table 3.8) (as required by DOE-STD-1020-2012, Section 4.3.2.4). Any point within the SRS domain can expect tornadic winds of about 75 mph every 1000 years, and winds of 260 mph every 10^8 years.

ANS-2.3-2011 lists the results of a PHA for tornadic winds in which the continental United States is subdivided into three broad regions, and separate statistics are calculated for each. The SRS lies within Region I (their Figure 1), which encompasses Illinois,

26

Arkansas, Missouri, Illinois, Iowa, and large parts of Texas, Oklahoma, Kansas, and Nebraska, which are all known to have heavy tornado activity. Table 3 of their report lists wind speeds of 170mph for 10^5 years, 200mph for 10^6 years, and 230mph for 10^7 years (Fig. 3.8). The corresponding values for our current analysis (calculated over the $2^0 \text{x} 2^0$ domain) are 147mph, 184mph, and 221mph, respectively, slower than those calculated over the larger, more active domain as expected.

Additionally, DOE (DOE-STD-1020-2012) guidelines (Section 4.3.2.8) require tornadic wind speeds for 3 return periods – 50,000 years, 125,000 years, and 10,000,000 years, and these are listed in Table 3.9. The latter return period is from Nuclear Regulatory Commission Regulatory Guide 1.76 (USNRC, 2007).
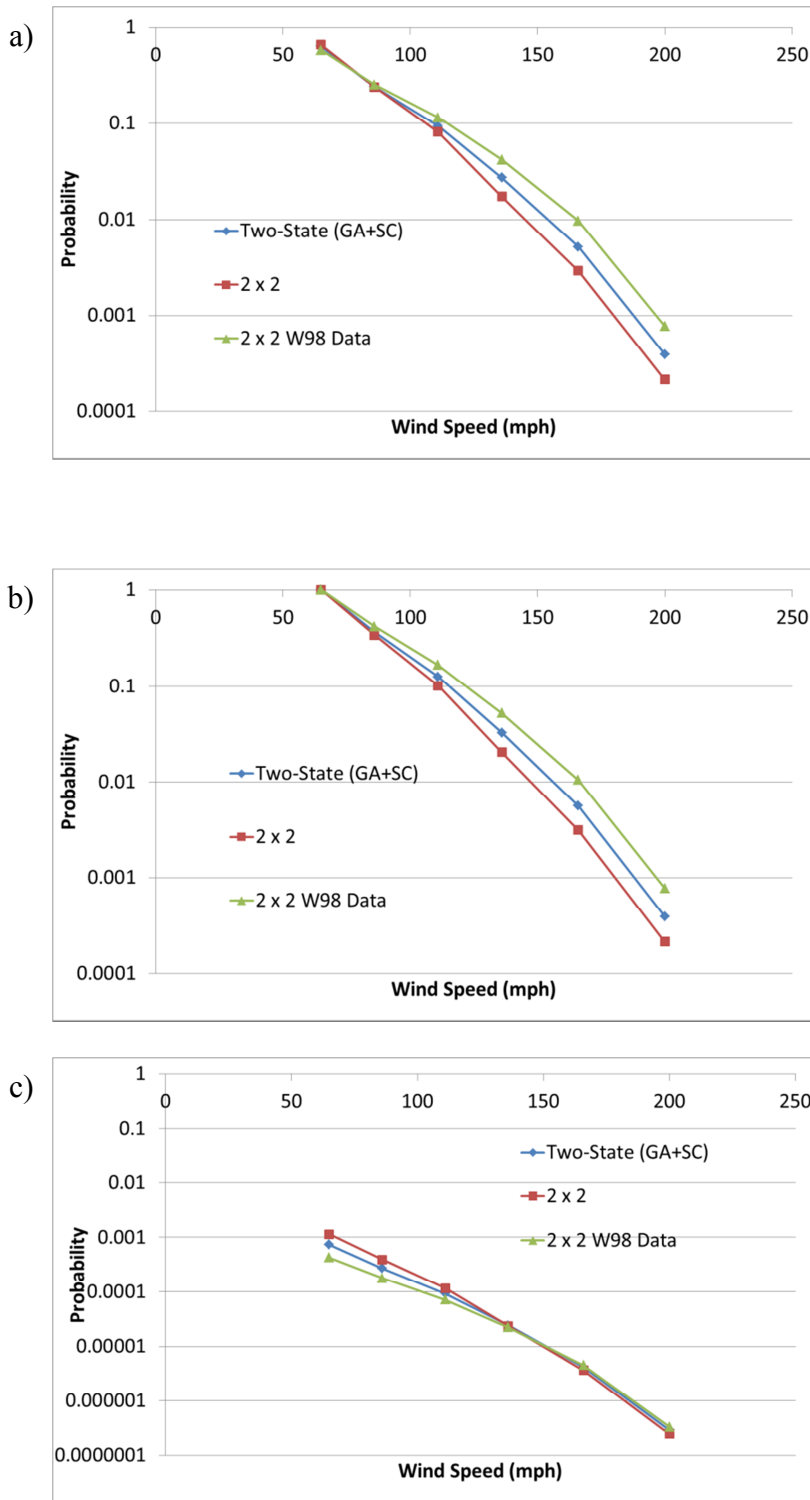
a)

b)

c)

Figure 3.7 a) The probability a point within a tornado path will have winds (3 second gust) at the given velocity, given that a strike occurs, b) the cumulative probability that any point within a strike will experience winds *above* that threshold, c) the probability (per year) that any point will experience winds at or above the given threshold.
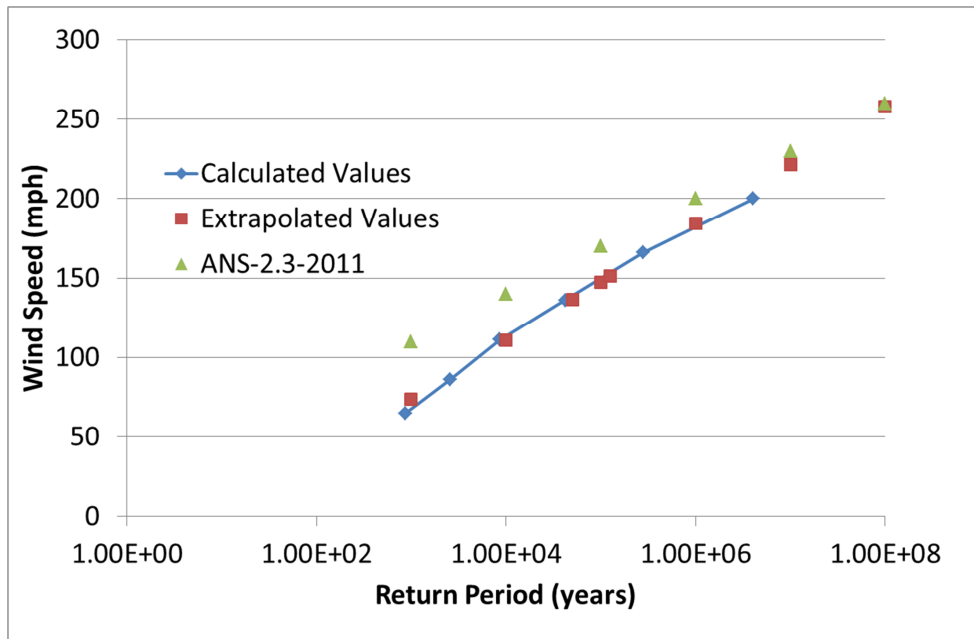
Figure 3.8 Tornadic wind speeds for the 2º x 2º domain corresponding to various return periods for both the values calculated from the observed tornadic wind speeds (with Eqs.1-4) (3 second gust), for a linear extrapolation of those values, and values from the ANS-2.3-2011 report.

Return Period (years)	Wind Speed (mph, 3 second gust)	Wind Speed (mph, 3 second gust), ANS-2.3-2011
1E+03	74	110
1E+04	111	140
1E+05	147	170
1E+06	184	200
1E+07	221	230
1E+08	258	260

Table 3.8 Expected wind speeds for various return periods.

Return Period (years)	Wind Speed (mph, 3 s gust)	Wind Speed (mph, 3 s gust), ANS-2.3-2011
50,000	136	161
125,000	151	173
10,000,000	221	230

Table 3.9 Tornadic wind speeds for DOE-mandated return periods.

4.0 Straight Winds

DOE-STD-1020-2012, Section 4.3.2.4 requires that sites develop a mean wind-related hazard curve (i.e., wind speed at the site as a function of mean return period in years). The ANS standard (ANS-2.3-2011, Section 3.4.2) specifies that a Fisher-Tippet Type I distribution be applied to estimate the wind risk probabilities for straight winds, but allows for the possibility of other, more suitable distributions if they can be demonstrated to be more applicable. Eliasson (1997) outlines a procedure for calculating the probability of extreme events by applying extreme value theory – the process of using existing data to create a probability function, then 'reading' the values at the tail of the function, which represent the largest, least likely values. We follow W98 and adapt Eliasson's (1997) algorithm for our purposes here, applying it to the longer datasets now available.

4.1 Wind Data

National Weather Service (NWS) wind gust data were analyzed for four sites in the vicinity of SRS: Augusta, GA, Macon, GA, Columbia, SC, and Athens, GA. Additionally, wind gust data were collected and analyzed from the CLM site near the center of SRS. Table 4.1 lists the locations and record lengths of the 5 sites. NWS wind gusts are defined as the peak three-second wind speed within each hour (Smith et al., 2003). Data were recorded over a period of four decades, allowing for a reasonable sample from which to derive the statistics.

To be recorded as a gust, an NWS wind reading must be sustained for either five seconds when recorded with an anemometer (prior to 2003), or for three seconds if recorded with an ultrasonic device (generally after 2003) (Smith et al., 2013). (The shorter period is required by ANS-2.3-2011, Section 3.4.1). Little difference was seen in wind speeds before and after instrument transitions were made (Smith et al., 2013), so we will not correct for this. Wind recorded at CLM is somewhat different – the 1Hz cup anemometer saves data in 1 second blocks, and *any* wind maximum within a 15 minute interval is recorded as the 'gust' reading for that time block. In practice, however, recorded gusts rarely last less than 1 second. This still allows fast but brief wind gusts to enter the record that is different from criteria at an NWS station, forcing the typical gust to be higher at CLM. It is difficult to devise a reasonable correction for this, so we will apply the algorithm to the data as is (as in W98) with the caveat that the wind gusts at the site tower are defined differently than at the NWS stations. A comparison of one-second SRS wind gust data to the NWS three-second data shows the former to not be out of line with the latter (Table 4.1), so we do not believe that we are introducing a great error to the statistics.

Station	No. of years	Mean Gust Speed (mph)	Std. Deviation of Gust Speed (mph)
Augusta	40 (1973-2012)	52.1	8.63
Athens	40 (1973-2012)	51.08	10.04
Columbia	40 (1973-2012)	53.8	9.5
Macon	40 (1973-2012)	56.07	13.2
CLM	23 (1990-2012)	55.87	13.7

Table 4.1 Wind station data, including mean and standard deviation of the annual maximum wind gusts at SRS and the NWS stations.

Another issue with the CLM data is that the anemometer is at four meters, while the standard for NWS stations is ten meters. This would cause the CLM data to have slower recorded speeds than the other stations (all else being equal). Using CLM wind data at four meters and from a second anemometer on the tower at 18 meters, we apply a logarithmic correction to obtain an estimate of the ten meter wind at the Climatology tower location (as per DOE-STD-1020-2012, Section 4.2.3.2.1).

One problem exists with the NWS wind data: for pragmatic and economic reasons, the 10m standard was not always followed (Weber, 2002). For the stations selected, the height tended to lie within the range of 6m to 11m. The 10m standard was not met until the mid-1990s. This would leave us with little data to use if we eliminated all data prior to this time, nor is a realistic correction possible with readings at only one level, so we elected to use this data as is. A time series of wind gusts does not show an obvious trend or change in variability at the time of the transition, so we do not believe that we are introducing any large error to the analysis.

We will use the NWS and CLM data to establish a relationship between the wind speed and the probability that such speeds have occurred (or will occur in the future) in the vicinity of SRS. We will first determine the statistical properties of various candidate functions, then select the one that best fits the data. Our goal is to calculate the expected maximum wind gust within a one-year period for various return periods, and we therefore require the annual maxima that have occurred. Following the strategy outlined by Eliasson (1997), the maximum wind speed from station (j) in year (i) is (x_{ij}) (e.g., Fig.

4.1a). Since the number of years available at any one station is usually insufficient to investigate the nature of the maxima, Eliasson (1997) regionally pools the data from multiple observation stations. The maxima data from each time series are standardized by subtracting the station mean ($\bar{x}_j$) and then normalizing by the station standard deviation (s_j) of the maximum wind gusts for station (j) (Fig. 4.1b):

$$\tau_{ij} = \frac{X_{ij} - \bar{X}_j}{s_j} \tag{7}$$

resulting in n_j standardized wind deviations for station j, $j = 1, 2, ..., k$. There are now several (k) ranked series of length n_j (one for each station j), each with zero mean and a standard deviation of one (Fig. 4.1b). These values of τ_{ij} represent a collection of standardized wind deviations, and we can use them to determine the shape of the distribution from which they were drawn.

The τ_{ij} values are pooled together and then sorted from smallest to largest. Label the first (smallest) τ_{ij} value in this sequence as $\tau_{(1)}$, the next (second largest) τ_{ij} value in this sequence as $\tau_{(2)}$, and so on where the largest of the τ_{ij} values in this sequence is $\tau_{(n_T)}$, where $n_T = \sum_{j=1}^{k} n_j$ are the total number of observations at all of the stations (Fig. 4.2). The parentheses around the subscript indicate that the subscript is the rank order of the sorted data set.
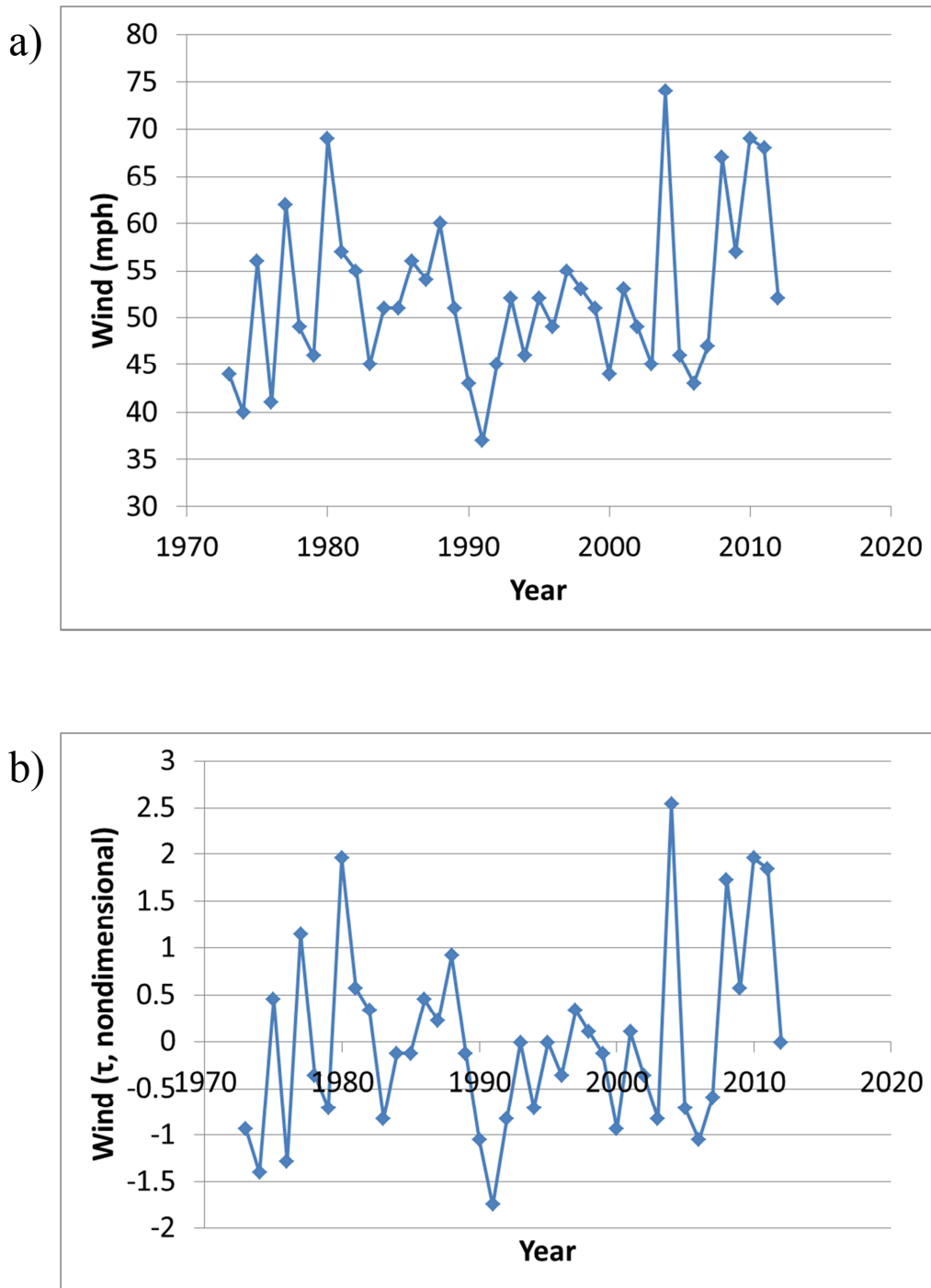
Figure 4.1 a) Annual wind gust maxima each year at Augusta, GA (NWS). b) As in a) but rendered nondimensional with the mean removed and normalized by the standard deviation (Eq. 7).
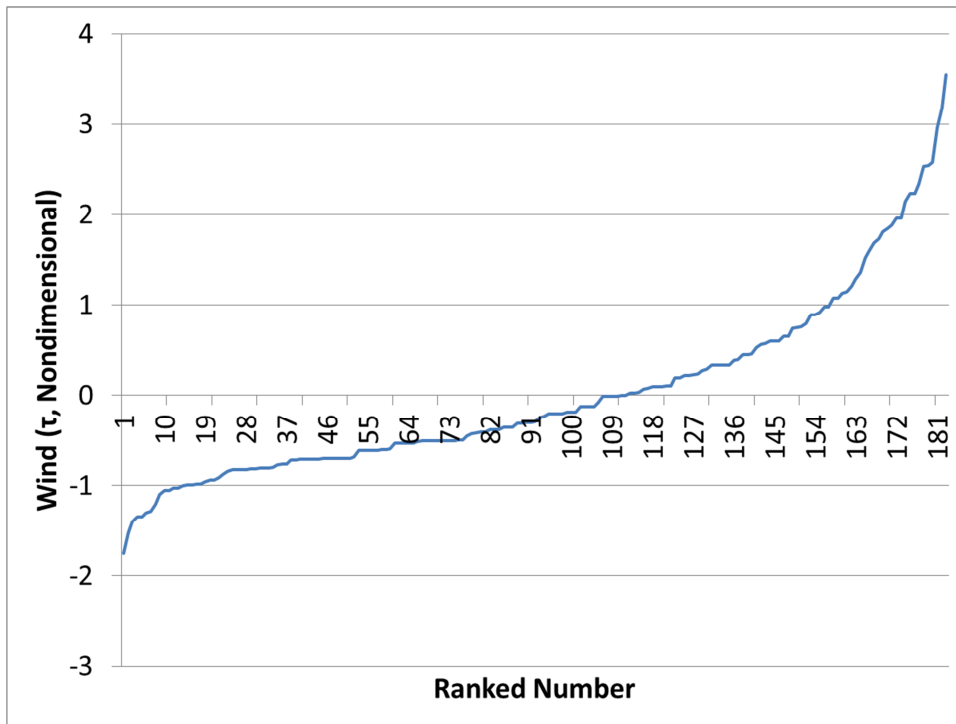
Figure 4.2 Ranked values of normalized wind maxima τ_{ij}.

4.2 Extreme Value Theory

The Fisher-Tippet, also known as generalized extreme value (GEV), distributions play an important role in modeling return periods [2] for maxima based on long series of observations, since it is the only possible limit distribution [3] for properly normalized sequences of maxima.

The maximal[4] GEV distribution was fit to the pooled standardized annual maximum wind deviations ($\tau_{(1)}, \tau_{(2)}, \ldots \tau_{(n_T)}$). From Castillo et al. (2005), the maximal GEV cumulative distribution function (CDF) is:

---

[2] A return period is the expected time until a specified threshold is exceeded.
[3] See Castillo and others [2005] for a general proof.
[4] Maximal refers to largest extreme values, the case of interest in this report. In contrast, a minimal GEV distribution refers to smallest extreme values, not considered here.

$$F(\tau;\xi,\alpha,\kappa) = \begin{cases} exp\left\{-\left[1-\kappa\left(\frac{\tau-\xi}{\alpha}\right)\right]^{1/\kappa}\right\}, 1-\kappa\left(\frac{\tau-\xi}{\alpha}\right) \geq 0, \kappa \neq 0 & \text{(8a)} \\ exp\left\{-exp\left\{\left(\frac{\xi-\tau}{\alpha}\right)\right\}\right\}, -\infty < \tau < \infty, \kappa = 0 & \text{(8b)} \end{cases}$$

where ξ is a location parameter that determines an offset value of the data, α is a scale parameter that helps determine the range of the data, and κ is a shape parameter, extremely important in determining the curvature of the CDF at the extreme values, as will be illustrated. The maximal GEV distribution can be partitioned into several special cases depending on the value of κ (Fig. 4.3a): the GEV Type 1 (GEV1, or a Gumbel) distribution occurs when $\kappa = 0$, the GEV Type 2 (GEV2, or Frechet) distribution occurs when $\kappa < 0$, and the GEV Type 3 (GEV3, or reverse Weibull) distribution occurs when $\kappa > 0$. The ordinate of the CDF plot (Fig. 4.3a) can be interpreted as the 'nonexceedance' probability, that is, the probability that a randomly selected wind (pooled standardized annual maximum wind deviation) value will be at or lower than specified value of τ in a given year. The value of the CDF monotonically increases as the specified value of τ increases, and experiencing wind values faster than τ becomes progressively less likely.
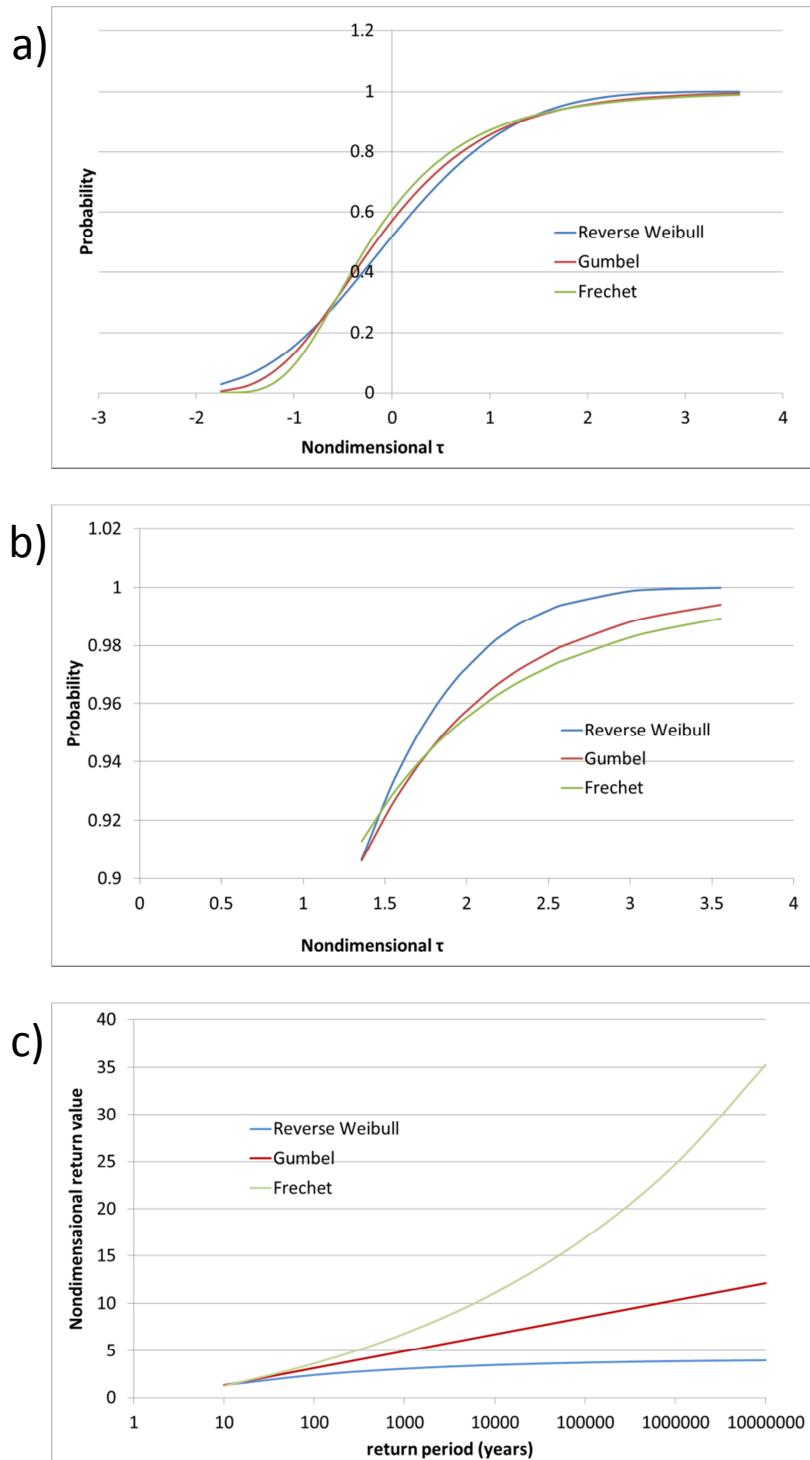
Figure 4.3 a) Nonexceedance probability curves for a Frechet (κ < 0), Gumbel (κ = 0), and reverse Weibull (κ >0) distribution. b) As in a), but above the 90th percentile. c) Return values for the three distributions.

At the extreme values (e.g., values of τ higher than 1.5), the Frechet distribution has lower nonexeedance probabilities than the Gumbel (Fig. 4.3b), making it *more* likely we will exceed any such value for τ. Conversely, the reverse Weibull distribution has higher nonexceedance probabilities (Fig. 4.3b), making large extremes *less* likely than a Gumbel distribution.

We can also calculate quantiles, for example, what wind speed value of τ is 99% likely to *not* be exceeded in a given year. Solving Eqs. 8 for τ, the *p*-th quantile for the maximal GEV distribution can be determined by

$$\tau_p = \begin{cases} \xi + \alpha[1 - (-\log p)^\kappa]/\kappa, \text{if } \kappa \neq 0 \\ \xi - \alpha\log(-\log p), \text{if } \kappa = 0 \end{cases} \tag{9}$$

where p is the probability of not exceeding a wind speed value of τ_p in a given year.

If T_τ is the time in years between successive events in which wind speed values are τ or greater, then the mean of T_τ is called the return period (RP_τ). Let $p = F(\tau; \xi, \alpha, \kappa)$ be the probability of not exceeding the wind speed value τ in a given year. If 1 - p is small, and the probability of more than one such event in a short duration is negligible, then the return period can be approximated by $RP_\tau \approx 1/(1 - p)$. For example, when p = 99%, the return period is approximately 100 years.

The GEV1 is the simplest of the three types. For GEV1 the return value curve is a straight line (Fig. 4.3c). The Frechet distribution has lower nonexeedance probabilities than the Gumbel (Fig. 4.3b), and the return value curve is therefore concave upward, yielding higher return values for any return period (Fig. 4.3c). Conversely, the reverse

Weibull distribution has higher nonexceedance probabilities (Fig. 4.3b) and the return period curve is concave downward. This distribution will therefore yield *lower* return values (Fig. 4.3c).

A technique for estimating κ by Hosking et al., (1985) is based on an approximate solution to a set of 'probability weighted moments'[5] (PWM). The sample PWMs are as follows (Hosking et al., 1985):

$$b_0 = \frac{1}{n_T}\sum_{i=1}^{n_T}\tau_{(i)} \tag{10a}$$

$$b_1 = \frac{1}{n_T(n_T-1)}\sum_{i=1}^{n_T}(i-1)\tau_{(i)} \tag{10b}$$

$$b_2 = \frac{1}{n_T(n_T-1)(n_T-2)}\sum_{i=1}^{n_T}(i-1)(i-2)\tau_{(i)} \tag{10c}$$

and the PWM estimator of κ is the solution to the following non-linear equation:

$$(3b_2 - b_0)/(2b_1 - b_0) = (1 - 3^{-\kappa})/(1 - 2^{-\kappa}). \tag{11}$$

Avoiding an iterative solution to Eq. 11, Hosking et al. (1985), notes that the right side of Eq. 11 is almost linear for $-0.5 < \kappa < 0.5$[6]. (Many hydrologic data sets are characterized by an even tighter range $-0.2 < \kappa < 0.2$, so this range for κ is not a practical limitation.) With this assumption, Hosking et al., (1985) derives the following closed-form approximate estimators:

$$c = \frac{2b_1 - b_0}{3b_2 - b_0} - \frac{log2}{log3} \tag{12}$$

$$\hat{\kappa} = 7.859c + 2.9554c^2 \tag{13}$$

---

[5] The traditional method of moments sets the first k moments of the theoretical distribution equal to their sample counterparts, and then solves the system of k equations to obtain estimates of the parameters. The probability weighted moments are a variation of this theme setting weighted theoretical moments equal to weighted sample moments, and then solving the system of equations to obtain estimates of the parameters.

[6] The interval $-0.5 < \kappa < 0.5$ was recognized by Hosking (1985) as a region in which the approximate estimator of κ was close to the value of the exact PWM estimator. When κ is not too far from zero, the PWM estimators enjoy the following advantages: feasible solutions, computing ease, and small biases unless the quantiles to be estimated are in the extreme tails of the GEV.

According to Hosking et al., (1985), the estimated value of κ from Eq. 13 can be judged by how well it satisfies the original non-linear Eq. 11. When using Hosking's linear approximation, the resulting error in κ is less than .0009 through the range $-.5 < \kappa < .5$ when compared to the iterative (exact) solution.

The estimated value of κ is used to determine which type of extreme value distribution to apply. Values close to 0 are indicative of the GEV1 (Gumbel) distribution (Eq. 8b), while, for values further away carry progressively less support. Deciding on which to use can be difficult as the existing data can be seen to fit either distribution equally well (Fig. 4.4a, b). According to Hosking et al., (1985), the estimator $\hat{\kappa}$ from Eq. 13 is asymptotically distributed as $N(0, 0.5633/n_T)$, where the sample size $n_T = \sum_{j=1}^{k} n_j$. We can determine an approximate 95% confidence interval for κ:

$$\left(\widehat{\kappa} - 1.645 \sqrt{\frac{0.5633}{n_T}}, \ \widehat{\kappa} + 1.645 \sqrt{\frac{0.5633}{n_T}} \right) \tag{14}$$

in order to get a better appreciation for the reliability of its estimate.

Another approach to identifying which special case of the GEV is applicable is to plot the idealized values assuming a particular limiting case such as the Gumbel distribution vs. the $\tau_{(i)}$ data series. First, Eqs. 8 are set to p, and then linearized as

$$-\ln(-ln(p)) = \frac{\tau_{(i)} - \xi}{\alpha}, \text{ for } \kappa = 0 \tag{15a}$$

$$(-ln(p))^{\kappa} = (1 - \frac{\kappa(\tau_{(i)} - \xi)}{\alpha}), \text{ for } \kappa \neq 0 \tag{15b}$$

A visual examination of fit of the theoretical vs. actual data values, and the calculation of Pearson's correlation coefficient r^2 between the theoretical left-hand side (LHS) and the

actual right-hand side (RHS) for the Eqs. 15 values is the primary tool used in this report to select a specific limiting distribution.

a)

b)
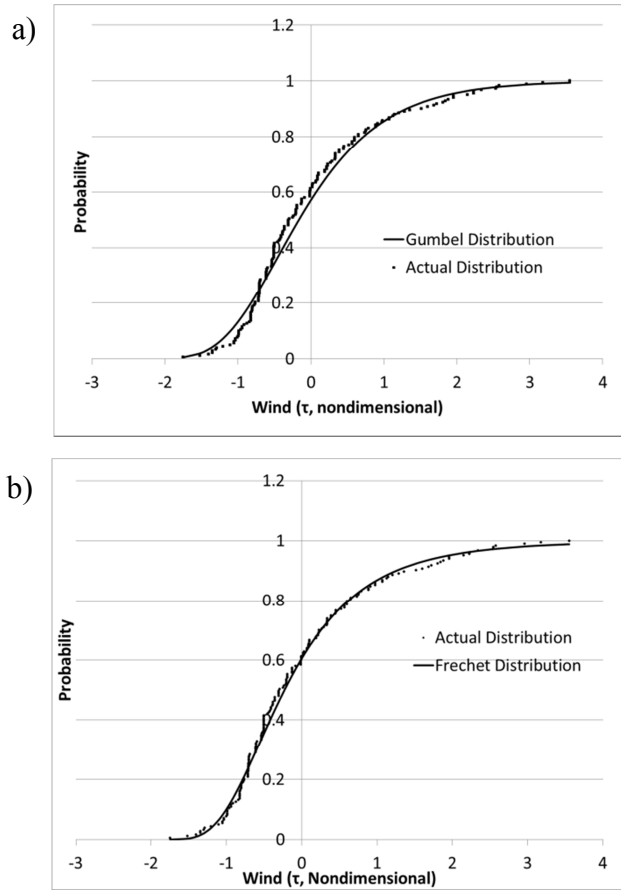
Figure 4.4 Comparison of the actual wind gust data distribution with the a) Gumbel and b) Frechet distributions.

If the Gumbel distribution is chosen, then the parameters ξ and α are determined by setting the mean of τ_{ij} to zero and the variance of τ_{ij} to one, resulting in constant values ($\alpha =.779697$, $\xi=-.45004$). If the Gumbel distribution is not chosen, we calculate ξ and α using the following equations from Hosking et al., (1985):

$$\hat{\alpha} = \frac{(2b_1 - b_0)\hat{\kappa}}{\Gamma(1+\hat{\kappa})(1-2^{-\hat{\kappa}})}$$ (16a)

41

$$\hat{\xi} = b_0 + \hat{a}\{\Gamma(1+\hat{\kappa}) - 1\}/\hat{\kappa}. \tag{16b}$$

To determine the wind speed for any return period, we assume that the curves in Eq. 8 represent the CDF. For any return period (e.g., $RP_{\tau_p} = 20$ years), the probability of non-exceedance (the probability that the time T_{τ_p} in years between events exceeds RP_{τ_p}) is

$$Prob\left(T_{\tau_p} => RP_{\tau_p}\right) = \left(1 - \frac{1}{RP_{\tau_p}}\right) = F(\tau_p) \tag{17}$$

(in this case, 95%). We then solve Eq. 8a or Eq. 8b for τ, using the values of ξ and α, and then restore the standard deviation and mean for each station according to the method outlined in Eliasson (1997). W98 outlines two procedures (one for $\kappa=0$, another for $\kappa\neq0$) for calculating the value of τ_p corresponding to a return period P, and converting that value of τ_p to an actual wind speed value.

For GEV1 or Gumbel distribution with a given return period RP_{τ_p}, the wind speed at Station j corresponding to a return period of RP_{τ_p} years is (W98):

$$X_{p_j} = s_j \left(-\ln\left[-ln\left\{\left(1 - \frac{1}{RP_{\tau_p}}\right)\right\}\right] - 0.57722\right)\left(\frac{1}{1.28255}\right) + \bar{X}_j \tag{18}$$

where the values 0.57722 and 1.28255 are from Eliasson (1997).

When calculating the values of X_{p_i} for a set of stations, we can get a smoother fit by applying the coefficients of variation of the respective stations (W98):

$$CV_j = \frac{s_j}{\bar{X}_j} \tag{19}$$

If we define $\overline{CV}$ as the average of CV_j values of all the k stations, W98 calculates the variable C_a as:

$$C_a = 0.78/\{\left(\tfrac{1}{\overline{CV}}\right) + 0.72\} \tag{20}$$

If we define X_5 as the 5-year return period value for a particular station j (calculated with Eq. 18), the wind speed value of X_P for any P value is then given as:

$$X_P = X_5[1 + C_a(y - 1.5)] \tag{21}$$

where

$$y = -\ln(-\ln\left(1 - \tfrac{1}{RP_{\tau_p}}\right)) \tag{22}$$

If we must apply a GEV2 or GEV3 distribution, we must solve for Eq. 8a for the wind speed τ. This gives us the wind speed value X_{p_j} associated with a return period of RP_{τ_p} years at Station j.

$$X_{p_j} = \begin{cases} \overline{X_j} + s_j(\hat{\xi} + \left(\tfrac{\hat{\alpha}}{\hat{k}}\right)(1 - y)) & \text{when } y \leq y_{lim_j} \\ x_{pm} > y_{\lim} & \text{when } y > y_{lim_j} \end{cases} \tag{23}$$

where

$$y = \left[-\ln\left(1 - \tfrac{1}{RP_{\tau_p}}\right)\right]^{\hat{k}} \tag{24}$$

and

$$y_{lim_j} = 10.7 - 0.007X_{5_j} \tag{25}$$

and X_{5_j} is the wind speed for the 5-year event.

4.3 Results for Wind Gusts

The Gumbel distribution is commonly used to fit a CDF to a ranked dataset, but this assumes a value of $\kappa=0$. If the value deviates substantially from that, a Frechet or reverse Weibull distribution would be more appropriate. We therefore require a method to decide which distribution to use, especially as the final values can be sensitive to the selected distribution. W98 accomplished this by applying a Z-score significance test (Eq. 14) to estimate if κ was significantly different from 0. For the current analysis, we apply a different method – fit the data to both distributions and compare the respective fits (Eq. 15). We can make the decision based on which fits better (or if no significant difference exists).

For the wind data, we obtain $\hat{\kappa}=-0.130258$. We see in Fig. 4.5a,b that the Gumbel distribution actually fits the data (slightly) better than the Frechet ($\kappa<0$), implying that the former is a more reliable predictor for extreme wind gust values. We therefore elect to use the Gumbel in our final analysis of this variable.
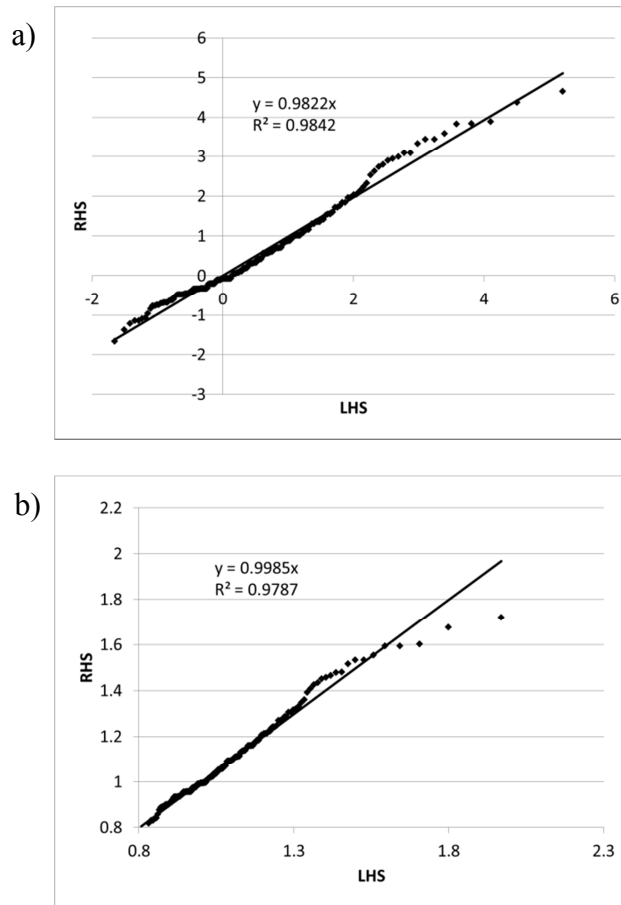
a)

b)

Figure 4.5 Comparison of the LHS and RHS of Eq. 15 for a) the Gumbel distribution, and b) the Frechet distribution.

We then apply Eq. 21 to the data and solve for X_P for each station, restoring each respective mean and standard deviation. The results for SRS (Table 4.2, Fig. 4.6) show that we may expect a sustained gust of ~70mph every 10 years, with a gust of ~160mph every 100,000 years, and these values are similar to those from the W98 report (which also used the Gumbel distribution for wind speeds). The values from ANS-2.3-2011 (Table 4.2) compare well with those from the current report (Fig. 4.6). As in Fig. 2 of W98, we plot this data (required by DOE-STD-1020-2012, Section 4.3.3.1) along with the tornadic wind probabilities from Section 3 (Fig. 4.7). We see that (as in W98) wind speeds for return periods less than about 500,000 years are actually faster for the straight

winds, but for periods longer than that, tornadic winds represent a larger hazard. DOE guidelines (DOE-STD-1020-2012, Section 4.3.2.8) also require wind speeds for 2 return periods – 2,500 years, and 6,250 years, and these are listed in Table 4.3.

Return Period (years)	Wind gust (mph), Current report	Wind gust (mph) from ANS-2.3-2011
10	72.6	76
100	94.0	96
1000	115.0	118
10000	136.0	137
100000	157.0	158

Table 4.2 Straight wind speeds for selected return periods.

Figure 4.6 Projected wind gust values for various return periods at SRS (from Eq. 21), along with the values from the W98 and the ANS-2.3-2011 reports.
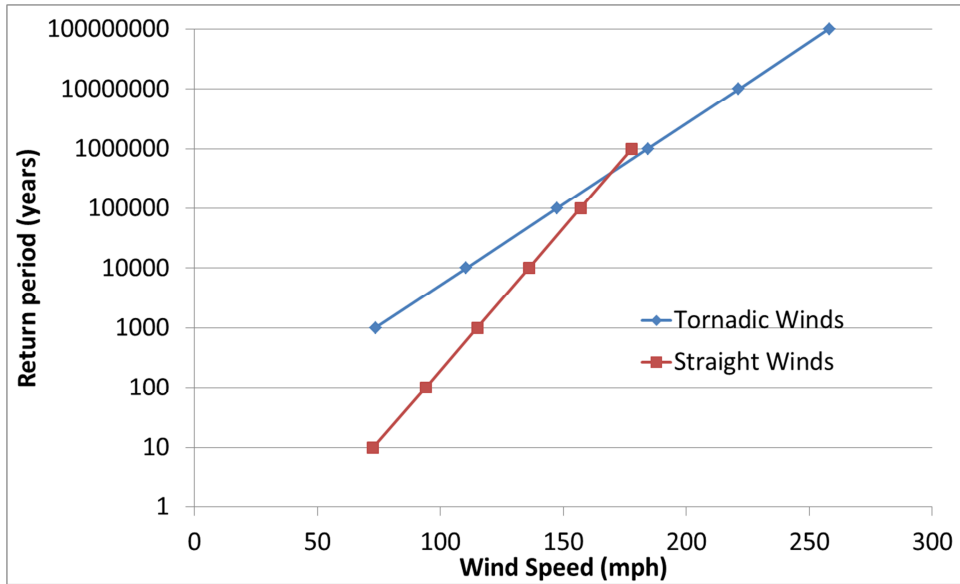
Figure 4.7 Comparison of tornadic and straight wind gust probabilities.

Return Period (years)	Wind gust (mph)	Wind gust (mph) ANS-2.3-2011
2500	123	125
6250	131	133

Table 4.3 Straight wind speeds for DOE-mandated return periods.

5.0 Precipitation

DOE-STD-1020-2012, Section 5.4.2.2.5 calls for 'stochastic methods' or 'probabilistic hydrologic modeling' to determine extreme precipitation frequency, and Section 7.4.2.1 again calls for the relationship between precipitation level and the design basis return period in years. As for the straight winds, extreme precipitation probability thresholds will be calculated with the algorithm of W98 - we will apply GEV1, 2, 3 distributions to the data, and 'read' the desired extreme values from the tails of the distribution. As before, we will start with a time series of the maximum precipitation total for each year, then calculate how likely *any* total is from that distribution. The relevant statistic with flood potential is how much rain falls within a short period, and W98 calculated probabilities for various such periods. We will adapt these same methods for our own calculation.

Precipitation records are collected at various frequencies, and we have data records at fifteen minute, hourly, and daily intervals – each of which represents the total precipitation that accumulated over that period. We can aggregate that data to get other desired periods.

5.1 Precipitation Data

We have assembled and collected precipitation data records from several locations, both on and off site. They were recorded at various intervals, and we must aggregate the data within each record to each desired accumulation period. On site, we have data recorded daily at eleven locations, with 15 minute data recorded at CLM (Table 5.1). We have

also collected offsite NWS data from seven regional weather stations. Of these, four are recorded every 15 minutes, while these and the other three are recorded hourly (Table 5.2).

Station	No. of years	Freq. of Observation
700-A	49	Daily
BARR2	41	Daily
BARR3	49	Daily
BARR5	43	Daily
100-C	29	Daily
400-D	40	Daily
200-F	49	Daily
200-H	29	Daily
100-K	29	Daily
100-L	34	Daily
100-P	45	Daily
CLM	11	15 Minutes

Table 5.1 Precipitation Data at SRS. Data was collected over the period from 1964 to 2012.

Station	No. of years	Freq. of Observation
WAGENER	39	15 Minutes
SYLVANIA	33	15 Minutes
LOUISVILLE	42	15 Minutes
CLARK HILL	34	15 Minutes
AUGUSTA	63	Hourly
ATHENS	55	Hourly
COLUMBIA	61	Hourly
WAGENER	60	Hourly
SYLVANIA	54	Hourly
LOUISVILLE	63	Hourly
CLARK HILL	61	Hourly

Table 5.2 National Weather Service precipitation data. Data was collected over the period from 1950 to 2012 for the hourly data and from 1971 to 2012 for the 15 minute data.

We will use the same accumulation periods as in W98 – 15 minutes, 1 hour, 3 hours, 6 hours, and 24 hours. For each period, we will calculate the annual maximum (e.g., the maximum 3 hour accumulation of each year), then apply the same algorithm in W98. Not all the stations can be used for every period. For the 15 minute accumulation period, we can only use the site data at CLM (Table 5.1) and the NWS data at Wagener, Sylvania, Louisville, and Clark Hill (Table 5.2). For the 1 hour period, we can use the CLM 15 minute datasets aggregated to 1 hour, plus hourly NWS data (Table 5.2). For the 24-hour accumulation period, we can use all the collected data.

W98 applies a correction to this data to account for the fact that a rainfall event may begin during one recording period and end during another, possibly forcing a strong event to be recorded as two weaker ones. This will have a stronger effect on shorter accumulation intervals, and W98 corrected for this with multiplication factors to be applied to each interval (Table 5.3). For the 15 minute interval, the recorded 15-minute data are multiplied by 1.13, while the data recorded hourly are multiplied by the same factor when the one hour interval is studied (Table 5.3). When the hourly and 15 minute data are aggregated to create three- and six-hour datasets, smaller factors are applied. For the 24-hour interval, the sub-daily recorded data are recorded by the small factor of 1.01, while the data recorded daily are multiplied by 1.13.

Accumulation Interval	Multiplication Factor
24 Hours	1.01/1.13
6 Hours	1.02
3 Hours	1.03
1 hour	1.13
15 Minutes	1.13

Table 5.3 Multiplication factors for Annual Maximum, as per W98.

5.2 Extreme Value Theory

Section 5.4 of DOE-STD-1020-2012 calls for probabilistic modeling of future precipitation totals. As with the wind data, we will take the time series of annual precipitation maxima and will use them to create a nonexceedance pdf by fitting the same distributions (Eqs. 8), then we will read the desired extreme values from the tail. The major difference is that we must repeat this for various accumulation periods. We first select an accumulation period, then aggregate (if required) the data at each station to match (e.g., calculate all one-hour accumulations from the 15 minute data (Fig. 5.1)). Then, we select the maximum value within each year. After this, we normalize the time series as in Eq. 7, and apply the same procedure to obtain the nonexceedance probability (Eqs. 8).
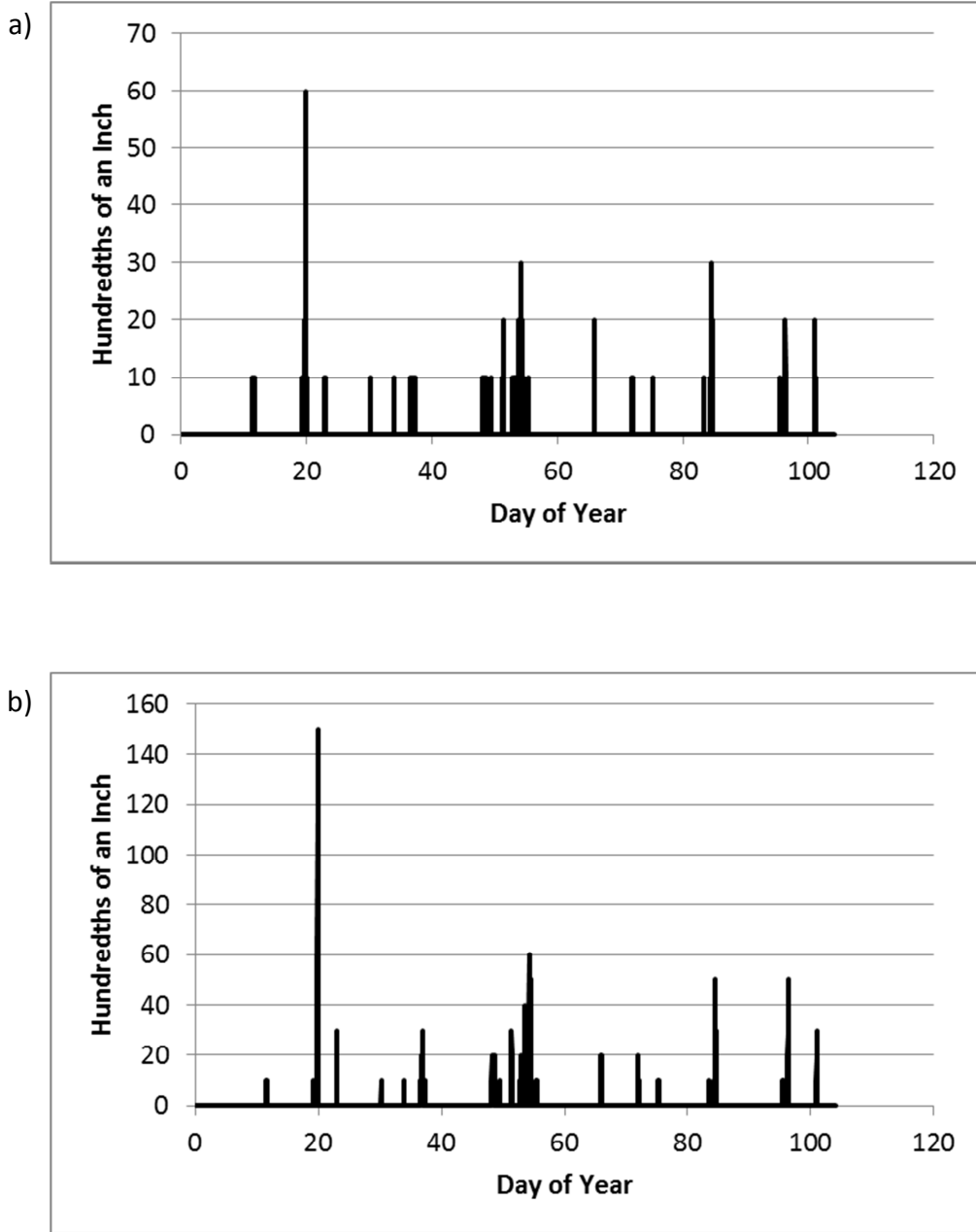
a)

b)

Figure 5.1 a) Time series of annual maximum 15-minute precipitation readings for the CLM for 1979. b) The same series, now aggregated to 1 hour accumulation periods.

5.3 Results for Precipitation

As described in Section 4.2, we will calculate the terms in Eqs. 15 and correlate the LHS and RHS of each to estimate the degree to which each distribution best fits the data.

Table 5.4 shows the correlation values, and one thing stands out - for all averaging periods except the 15 minute precipitation, the GEV1 (Gumbel) correlation is higher than or within 1% of the GEV2 (Frechet) or GEV3 (reverse Weibull), in agreement with the generally low values of κ. For this reason, we will apply the Gumbel curve when calculating these precipitation extremes. For the 15 minute precipitation, with its higher κ value, the correlation for the reverse Weibull ($\kappa > 0$) is about 1.5% greater than that for the Gumbel, exceeding the level of statistical significance. However, this distribution produces a curve that bends to the right, producing lower values than the Gumbel distribution. Given the small difference and the desire to maintain a conservative estimate, we will in this instance also use a Gumbel distribution to forecast the future precipitation probabilities.

	κ	Eq. 15a	Eq.15b
15 Minutes	.210	.981	.996
1 Hour	.043	.995	.996
3 Hours	-.045	.992	.994
6 Hours	-.067	.992	.994
24 Hours	-.038	.969	.967

Table 5.4 Correlation values between the LHS and RHS of Eqs. 15.

For the 15 minute accumulation period, we are limited to only five datasets (Table 5.5), with annual maximum averages that vary from ~0.75"-0.96". The projected accumulation totals (Fig. 5.2) vary from between 1-1.5" for a 10-year period, to about 3.0" for 10^5 years, about an inch lower than in W98.

Station	Average Peak Rainfall (inches)	Std. Deviation of Peak Rainfall (inches)
SRS	0.80	0.20
Clark Hill	0.79	0.21
Louisville	0.86	0.21
Sylvania	0.93	0.35
Wagener	0.84	0.29

Table 5.5 Data for the annual maxima for 15-Minute accumulated precipitation, calculated according to Eq. 21.
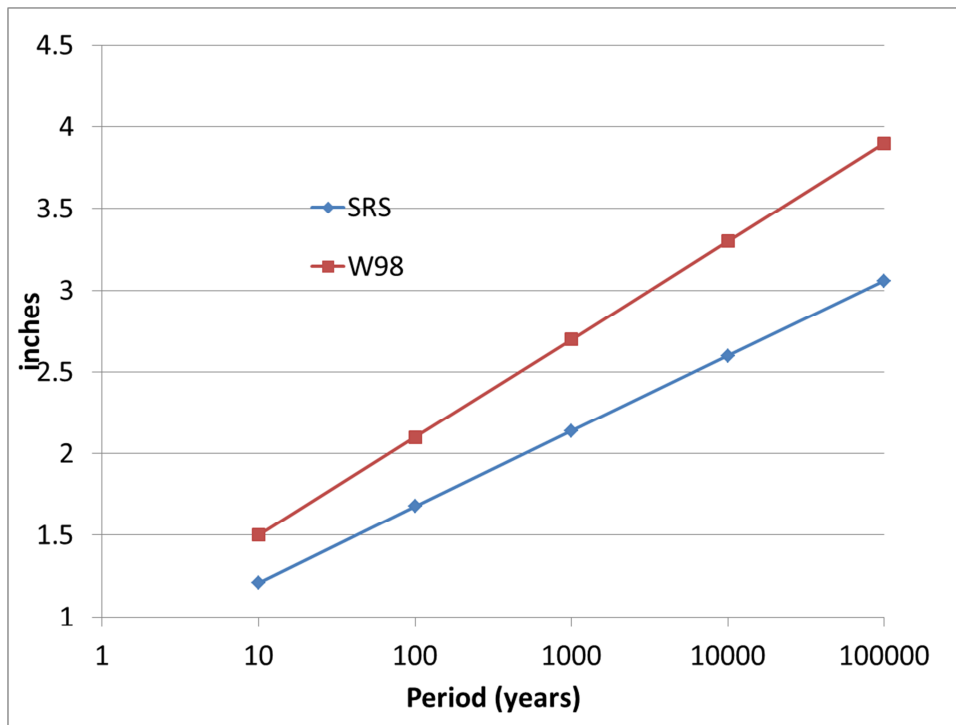

Figure 5.2 Projected 15-minute precipitation totals for various return periods at SRS, along with values from the W98 report.

For a one-hour period, we can now include the NWS stations recorded hourly in the data (Table 5.6), and see the averages range from about 1.35" to 1.65". The expected accumulations (Figure 5.3) generally range from about 2.5" for a 10 year period to 7" for 10^5 years (similar to W98).

Station	Average Peak Rainfall (inches)	Std. Deviation of Peak Rainfall (inches)
SRS	1.53	0.50
Clark Hill	1.54	0.81
Louisville	1.53	0.59
Sylvania	1.59	0.61
Wagener	1.57	0.56
Athens	1.52	0.55
Augusta	1.35	0.35
Columbia	1.65	0.58

Table 5.6 Data for the annual maxima for the 1-hour accumulated precipitation.
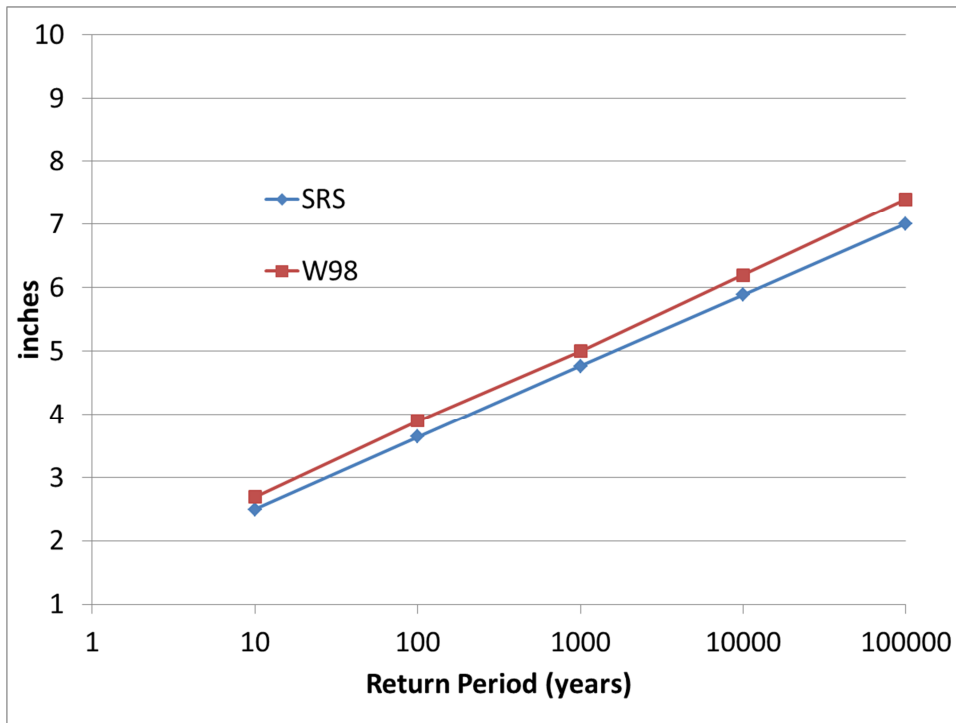

Figure 5.3 Projected 1 hour accumulation totals for various return periods at SRS, along with values from the W98 report.

When the data from the same stations used previously are aggregated to three-hour accumulation periods before creating a time series of the annual maximum of each year, the averages range from 2.1"-2.3" (Table 5.7). SRS can expect to see more than 9" every 10^5 years within a single 3-hour period (Figure 5.4).

Station	Average Peak Rainfall (inches)	Std. Deviation of Peak Rainfall (inches)
SRS	2.23	0.63
Clark Hill	2.11	1.02
Louisville	2.14	0.83
Sylvania	2.28	0.85
Wagener	2.15	0.82
Athens	2.15	0.75
Augusta	2.16	0.74
Columbia	2.29	0.86

Table 5.7 Data for the annual maxima for the 3-hour accumulated precipitation.

Figure 5.4 Projected 3 hour accumulation totals for various return periods at SRS, along with values from the W98 report.

Extending the period to six-hours (Table 5.8), averages now range from 2.5"-2.7".

We can now expect >~10" every 10^5 years (Fig. 5.5). If we want 24-hour accumulations, we must now include the SRS data from Table 5.1, and the station averages now range from about 3.0" to 3.7" (Table 5.9). With this data, we can expect values of ~5" every 10 years, with over 12" every 10^5 years (Fig. 5.6).

Station	Average Peak Rainfall (inches)	Std. Deviation of Peak Rainfall (inches)
SRS	2.66	0.67
Clark Hill	2.50	1.18
Louisville	2.57	1.03
Sylvania	2.62	0.93
Wagener	2.49	0.93
Athens	2.53	0.82
Augusta	2.63	0.99
Columbia	2.62	0.97

Table 5.8 Data for the annual maxima for the 6-hour accumulated precipitation.

Station	Average Peak Rainfall (inches)	Std. Deviation of Peak Rainfall (inches)
SRS	3.33	0.89
Clark Hill	3.52	1.52
Louisville	3.50	1.21
Sylvania	3.47	1.17
Wagener	3.20	1.06
Athens	3.40	1.18
Augusta	3.78	1.36
Columbia	3.46	1.12

Table 5.9 Data for the annual maxima for the 24-hour accumulated precipitation.

Station	Average Peak Rainfall (inches)	Std. Deviation of Peak Rainfall (inches)
700-A	3.24	1.17
BARR2	3.31	0.92
BARR3	3.16	0.89
BARR5	3.36	1.12
100-C	3.04	0.94
400-D	3.29	1.04
200-F	3.31	0.95
200-H	3.41	0.93
100-K	3.44	1.11
100-L	3.40	1.14
100-P	3.13	1.02

Table 5.9 continued

Figure 5.5 Projected 6 hour accumulation totals for various return periods at SRS, along with values from the W98 report.
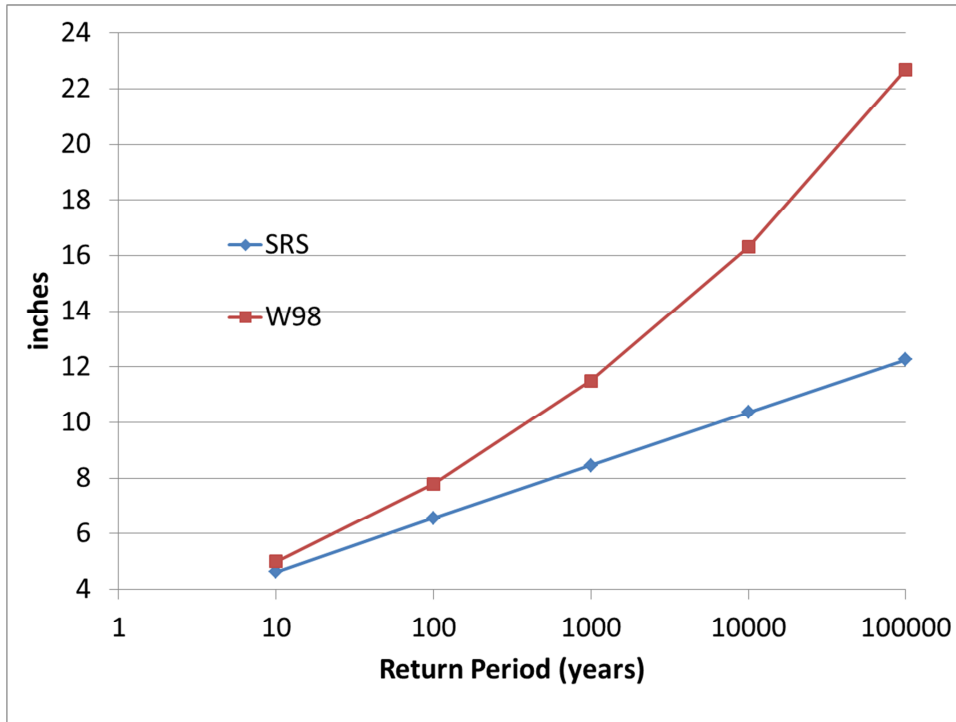
Figure 5.6 Projected 24 hour accumulation totals for various return periods at SRS, along with values from the W98 report.

Figs. 5.4-5.6 reveal large differences between the values from W98 and the current values for the 3hr-24hr accumulation periods. This is largely a consequence of the W98 values for κ, which were often 2-3 times the values calculated here ($\sim$ -0.1 to -1.3), forcing the use of a Frechet distribution with its corresponding higher extreme probabilities. (For our values, the values of κ were low to the point that the use of the Gumbel and Frechet distributions produced nearly identical values for the 3-24 hour accumulation periods.) The calculation of κ is rather sensitive to the values of b_1, and b_2. As datasets get progressively longer with each version of the PHA, differences with each previous version should become less significant.

DOE-STD-1020-2012, Section 7.4.2.3 also requires precipitation amounts for four return periods – 2,500 years, 6,250 years, 10,000 years, and 25,000 years, and these are listed in Table 5.10 for the different accumulation periods. For more extreme rainfall events, DOE (2012) defers to commercial industry practice. The NRC requires nuclear power plants to be designed based on a flood (design basis flood) produced by the probable maximum precipitation (PMP) storm, which is defined as the greatest rainfall theoretically possible over given duration intervals and river basin drainage areas (USNRC, 1977). Maps of PMP for rainfall durations from 6 hr to 72 hr and drainage areas from 26 km^2 to 20,000 km^2 are given in Schreiner and Riedel (1986). For SRS, the PMP for 6-hr and 24-hr duration events for a drainage area of 518 km^2, the approximate area of the Upper Three Runs Creek basin, were estimated from the appropriate maps. These values are listed in Table 5.10.

Return Period (years)	15 Minutes	1 hour	3 hours	6 hours	24 hours
2500	2.32	5.21	6.75	7.78	9.22
6250	2.50	5.66	7.33	8.44	9.97
10,000	2.60	5.89	7.63	8.78	10.36
25,000	2.78	6.33	8.21	9.44	11.11
PMP*				22.9	34.5

Table 5.10 Peak precipitation values (inches) for DOE-mandated return periods.

6.0 Quality Assurance

To ensure the accuracy of the reported methods and results, an independent review was performed. This review examined written calculations, computer programs and Microsoft Excel® charts for proper equations and consistency between the different formats.

Meteorological data taken from sources located onsite at SRS have previously undergone quality assurance review and are deemed acceptable for use in this report. Datasets obtained from the NCDC should already have undergone quality control as well for removal of bad data points. Missing data in these datasets was replaced with zeroes and were mainly used to ensure proper processing of the dataset. The primary difficulties in compiling the tornado set are the differences in reporting between datasets and the differences in tornado classification before and after 2007. These were addressed using methods published in peer-reviewed articles.

Methods for calculating the return periods and extreme value theory used for straight winds and precipitation are grounded in peer-reviewed literature and regulatory documents from DOE. Analysis of the hand-calculations confirms that these methods are being properly computed. The results are sound and fit within expected ranges based on the available data.

Based on the independent review, it was determined that the reported methodology agreed with the procedures used by the authors. Further, no mistakes were found in the authors' calculations.

7.0 References

American National Standard, 2010: *Determining Meteorological Information at Nuclear Facilities*, ANSI/ANS-3.11-2005, American Nuclear Society, La Grange Park, IL (2010).

American National Standard, 2011: Estimating Tornado, Hurricane, and Extreme Straight Line Wind Characteristics at Nuclear Facility Sites, ANSI/ANS-2.3-2011, American Nuclear Society, La Grange Park, IL (2011).

Boissonnade, A., Q. Hossain, J. Kimball, R. Mensing, and J. Savy, 2000: Development of a Probabilistic Tornado Wind Hazard Model for the Continental United States Volume 1: Main Report, UCRL-ID-140922-VOL-1

Castillo, E., A.S. Hadi, N. Balakrishnan, and J. M. Sarabia, 2005: Extreme Value and Related Models with Applications in Engineering and Science, John Wiley & Sons, Hoboken, New Jersey.

Eliasson, J., 1997: A statistical model for extreme precipitation, *Water Resources Research*, **33**, 449-455

Hosking, J., J. Wallis, E. Wood, 1985: Estimation of the Generalized Extreme-Value Distribution by the Method of Probability-Weighted Moments, *Technometrics*, **27**, 251-261

Lu, D., 1995: A Statistically Rigorous Model for Tornado Hazard Assessment, Institute for Disaster Research, Master Thesis, Texas Tech University

McDonald, J. R., 1981: A Methodology for Tornado Hazard Probability Assessment, Prepared for Division of Health, Siting and Waste Management Office of Nuclear Regulatory Research, U. S. Nuclear Regulatory Commission, Washington, D.C.

Ramsdell, R., and J. Rishel, 2007: Tornado Climatology of the Contiguous United States, PNNL, NUREG/CR-4461, Rev. 2

Reinhold, T. A., and B. Ellingwood. 1982. Tornado Damage Risk Assessment. NUREG/CR-2944, U.S. Nuclear Regulatory Commission, Washington, D.C.

Savannah River Nuclear Solutions, The SRS Environmental Monitoring Plan, SRNS-TR-2012-00202

Schreiner, L., and J. Riedel, 1986: Probable Maximum Precipitation Estimates, United States East of the 105th Meridian, Hydrometeorological Report No. 51, U. S. Department of Commerce, Washington, DC

Scott, K. E., 2013: Savannah River Site Annual Meteorology Report for 2012, SRNL-RP-2013-00070, Savannah River National Laboratory, Aiken SC.

Smith, B., T. Castellanos, A. Winters, C. Mead, A. Dean, R. Thompson, 2013: Measured Severe Convective Wind Climatology and Associated Convective Modes of Thunderstorms in the Contiguous United States, 2003–09. *Wea. Forecasting*, **28**, 229–236.

United States Census Bureau, Summary of 2000 Census

USDOE, 2011: Radiation Protection of the Public and the Environment, DOE Order 458.1, Washington DC.

USDOE, 2004: *Environmental Regulatory Guide for Radiological Effluent Monitoring and Surveillance*, DOE-EH/0173T, Washington, DC (2004).

USDOE, 2012: Natural Phenomena Hazards Analysis and Design Criteria for DOE Facilities, DOE-STD-1020-2012, Washington, DC.

USNRC, 1977: Design Basis Floods for Nuclear Power Plants, Regulatory Guide 1.59, Washington, DC.

USNRC, 2007: Design-Basis Tornado and Tornado Missiles for Nuclear Power Plants.

Weber, A., 2002: Wind Climate Analyses for National Weather Service Stations in the Southeast (U), WSRC-TR-2002-00515

Weber, A. H., J. H. Weber, M. J. Parker, C. H. Hunter, and C. O. Minyard, 1998: Tornado, Maximum Wind Gust, and Extreme Rainfall Event Recurrence Frequencies at the Savannah River Site, WSRC-TR-98-00329.

Westinghouse Savannah River Company, 2004: Savannah River Site DSA Support Document – Site Characteristics and Program Descriptions, WSRC-IM-2004-00008.

Distribution:

B. J. Gutierrez (DOE-SR), 707-H
L. M. Chandler, 773-A
G. S. Elchoufi, 730-2B
D. D. Niehoff, 730-2B
C. H. Hunter, 773-A
R. L. Buckley, 773-A
S. R. Chiswell, 773-A
R. J. Kurzeja, 773-A
M. J. Parker, 773-A
K. E. Scott, 773-A
B. J. Viner, 773-A